

**Report on the Design, Development and Test of a
C-Band Flight Thruster**

September 2010

Issue 2. December 2017

The copyright in this document is the property of Satellite Propulsion Research Ltd.

This document contains PROPRIETARY INFORMATION, which must not be disclosed without prior approval.

CONTENTS

1. Introduction
2. Flight Thruster Design
 - 2.1 General Description
 - 2.2 Electrical Design
 - 2.3 Mechanical Design
3. Development Programme
 - 3.1 Equipment Specification
 - 3.2 Flight Electrical Model (FEM)
 - 3.3 Flight Test Model (FTM)
4. Test Bench
 - 4.1 Microwave equipment
 - 4.2 Force Measurement Rig
 - 4.3 Instrumentation
 - 4.4 EMC and Safety
5. Test Procedures
 - 5.1 Tuning and Q Measurement
 - 5.2 Power Measurement and Calibration
 - 5.3 Frequency Tracking
 - 5.4 Force Measurement and Calibration
 - 5.4.1 Force Measurement Principles
 - 5.4.2 Rig Calibration
 - 5.4.3 Test Run Procedure
 - 5.5 Temperature Measurement
6. Test Results
 - 6.1 Specific Thrust
 - 6.2 Reaction Force Plots and Analysis
 - 6.3 Resonant Frequency Tracking Results
 - 6.4 Thermal Results and Analysis
7. Test Summary and Conclusions
8. Appendix A

FIGURES

- 1.1 Flight Test Model Thruster

- 2.1 Block diagram of Flight Engine
- 2.2 E Field Phase Response
- 2.3 H Field Phase Response
- 2.4 FTM Impedance Plot
- 2.5 FTM General Arrangement Drawing
- 2.6 Effect of Machining Tolerance

- 3.1 Flight Electrical Model Thruster

- 4.1 General view of Test Bench
- 4.2 Block diagram of Test Bench
- 4.3 Diagram of Force Measurement Rig
- 4.4 Force Measurement Rig
- 4.5 Diagram of Free waveguide coupling

- 5.1 FTM Resonant Frequency Plot
- 5.2 Pmon Calibration
- 5.3 Pdet and Prefl Calibration
- 5.4 Frequency track for Medium Power Test Run
- 5.5 Thruster force diagram
- 5.6 Test Run Simulation
- 5.7 Spring and Balance calibrations
- 5.8 Force Measurement Rig calibration
- 5.9 Test FTM 177 Spurious Force

- 6.1 Thrust Data for Performance Tests
- 6.2 FTM 169 Test Results
- 6.3 Loaded and Unloaded Q
- 6.4 Thrust/Pdet ratio Plot
- 6.5 FTM 157 Test Results
- 6.6 FTM 174 Test Results
- 6.7 FTM 174 Test Results
- 6.8 Temperature Change Data for FTM 154
- 6.9 Baseplate Thermal Results
- 6.10 Wall Temperature/Resonant Frequency Plot

TABLES

- 1. FTM Electrical Design Summary
- 2. Test Equipment list
- 3. Microwave Power Levels and Losses
- 4. Frequency tracking algorithms
- 5. Performance test results
- 6. Test results summary

Proprietary Information

1. Introduction

This document reports on the design, development and test of the SPR Ltd C-Band Flight Thruster, shown in Fig 1.1. The programme ran from October 2008 through to September 2010. The majority of the work was carried out under private investment funding and shareholder loans, with a small part of the test programme funded under Boeing Purchase Contract No 9CS114H.

Issue 2 of this document includes minor updates and editorial corrections together with Appendix A, which contains the original manufacturing drawings.



Fig 1.1 Flight Test Model Thruster

2. Flight Thruster Design

2.1 General Description

The thruster operates at 3.85 GHz, with a specified output of 85 mN for 300 W microwave input. It is designed to operate from two 150 W flight qualified TWTAs, and a Frequency Generator and control unit (FGCU), as shown in the block diagram in fig 2.1.

The thruster is designated a Flight Test Model (FTM). Substituting the present commercial connectors with flight qualified items, and employing

Proprietary Information

space QA procedures during the manufacture, would enable the design to proceed to a full flight qualification programme.

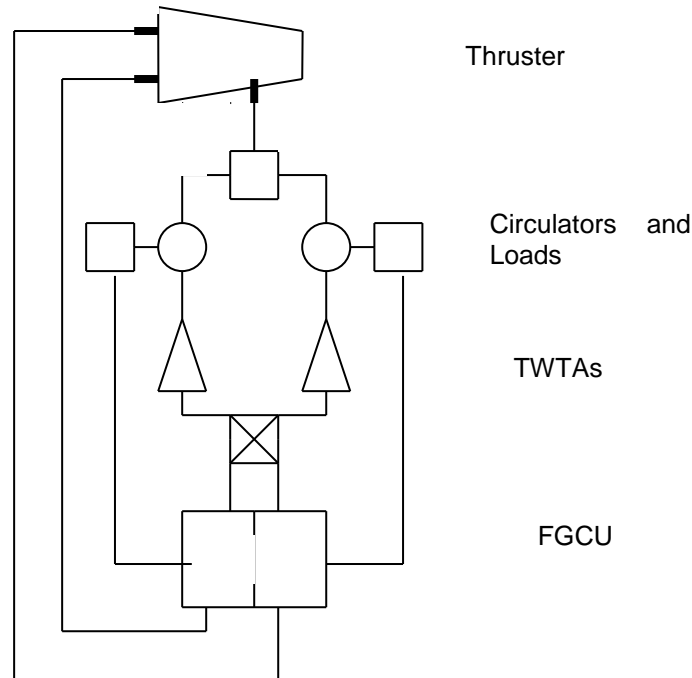


Fig 2.1 Block Diagram of Flight Engine

2.2 Electrical Design

The basic cavity design was carried out using SPR proprietary design software. This enables the cavity geometry and dimensions to be calculated, together with impedance and position of the input and detector circuits. Theoretical, unloaded Q can be calculated, together with the predicted frequency shift under temperature change.

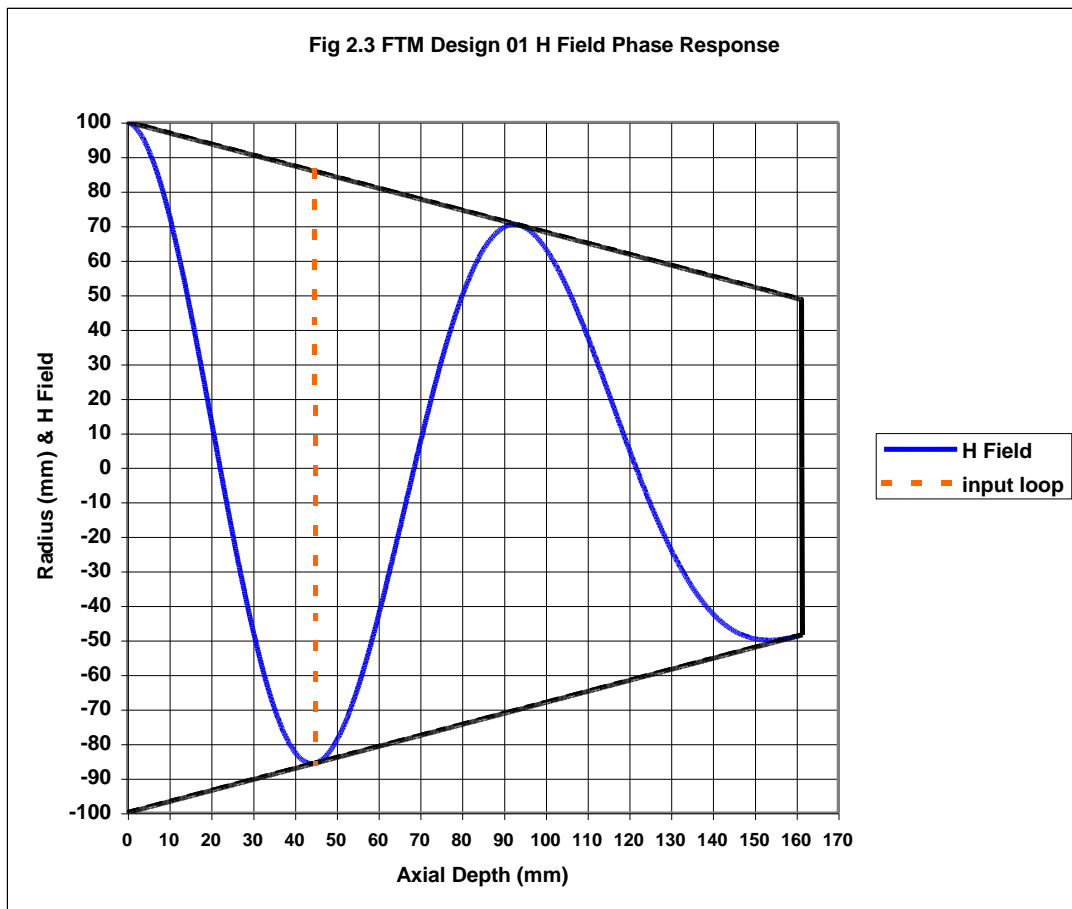
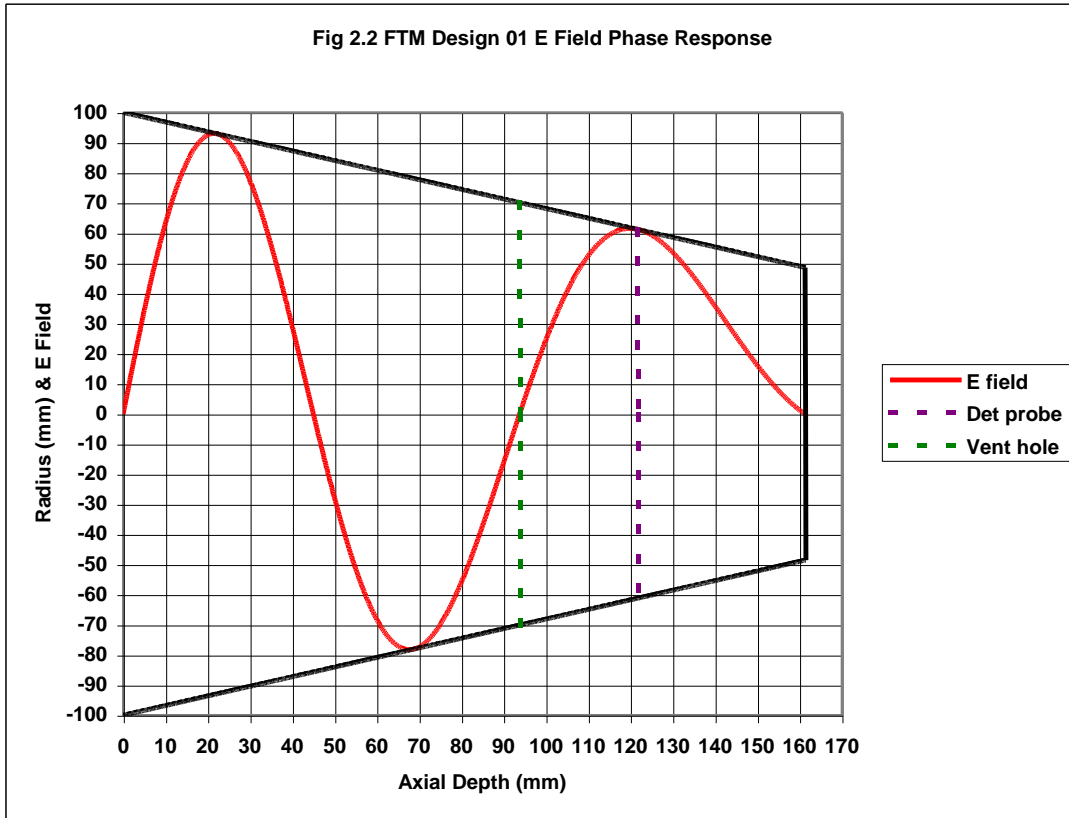
The design is summarised in the output file given in Table 1, together with the E and H field plots given in Figs 2.2 and 2.3, and the Impedance plot in Fig 2.4.

Proprietary Information

| Design Summary FTM 01.3 | | | |
|-----------------------------------|---------------------------------|-------|--|
| | | | |
| Thruster Model | FTM Drawing FTM1 002 issue 1 | | |
| Analysis File | FTM design 01.3 | | |
| File Date | 06-Sep-10 | | |
| Input Data | Input Data shown | | |
| Cavity Geometry | Circular | | |
| Environment | Air | | |
| Major Dimension D1 | 200 | mm | |
| Minor Dimension D2 | 97 | mm | |
| Taper Length L1 | 161.5 | mm | |
| Cone Angle | 17.69 | deg | |
| Propagation Mode | TE01 | | |
| p | 3 | | |
| Resonant Frequency | 3873.6 | MHz | |
| Major Guide Wavelength | 87.75 | mm | |
| Minor Guide Wavelength | 333.61 | mm | |
| Design Factor | 0.8168 | | |
| Cut-off diameter | 94.36 | mm | |
| Cut-off frequency @ D2 | 3767 | MHz | |
| Input Position | 45 | mm | |
| Input Impedance | 314.4 | Ohms | |
| Detector Position | 121.8 | mm | |
| Detector Impedance | 239.6 | Ohms | |
| Cavity Material | Silver plated aluminium | | |
| Theoretical Unloaded Q | 73,243 | | |
| Theoretical Maximum Static Thrust | 399 | mN/kW | |
| Unloaded 3dB bandwidth | 53 | kHz | |

Table 1. FTM Electrical Design Summary

Proprietary Information



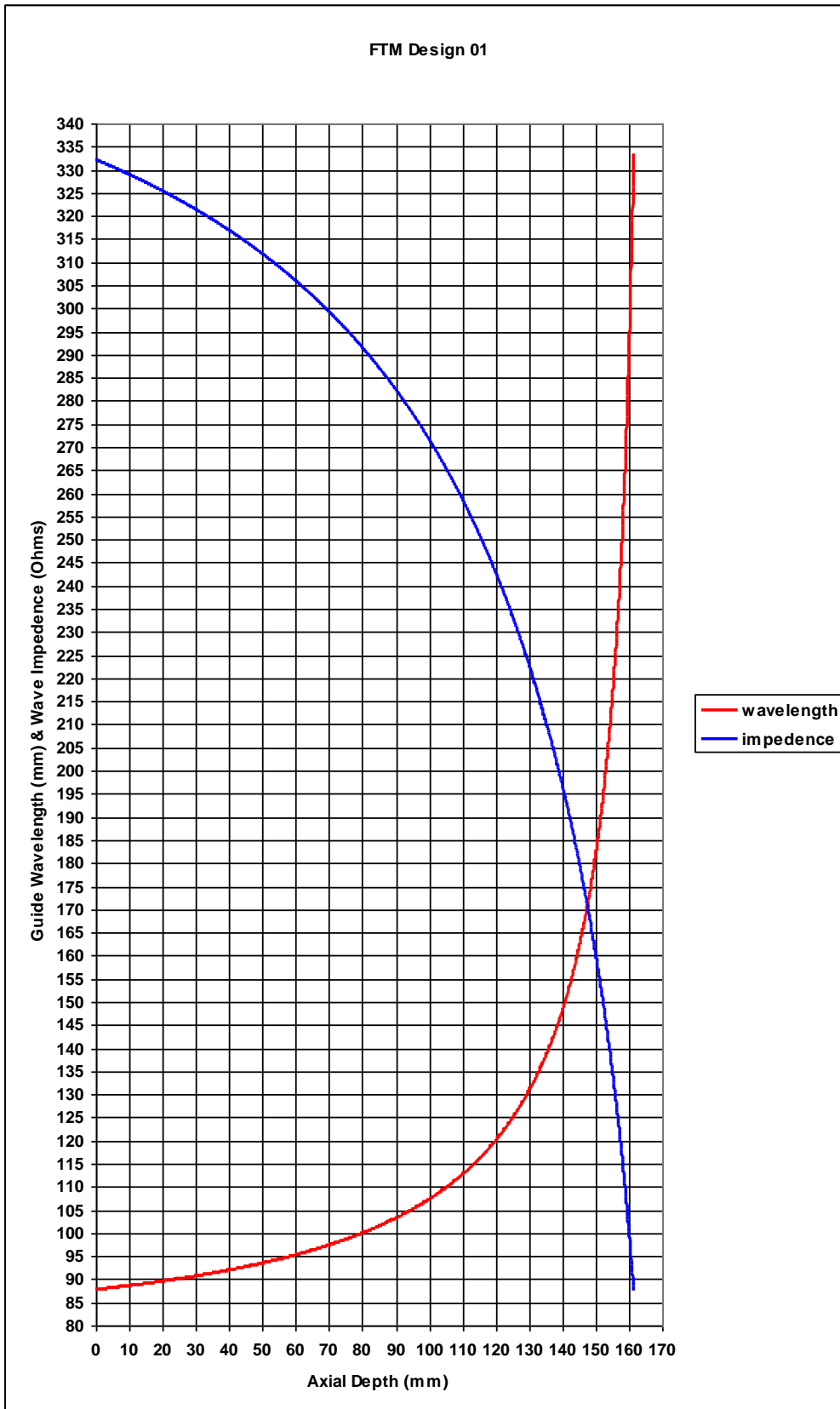


Fig 2.4 FTM Impedance Plot

Proprietary Information

2.3 Mechanical Design

The thruster cavity is machined from an AlMgSi 6061 alloy, and is assembled from 3 main components, baseplate, body and top plate. These are fixed by a total of 72 socket headed M4 screws. The flange thickness and flatness ensures good EMC performance. The input circuit is a loop design, based on an N type connector. A tuning screw is mounted adjacent to the loop, to provide resonance tuning of the input circuit. A detector probe is provided to monitor cavity resonance, and is assembled from an SMA connector. The thruster is illustrated in Fig 2.5.

The measured mass of the thruster is 3.193 kg.

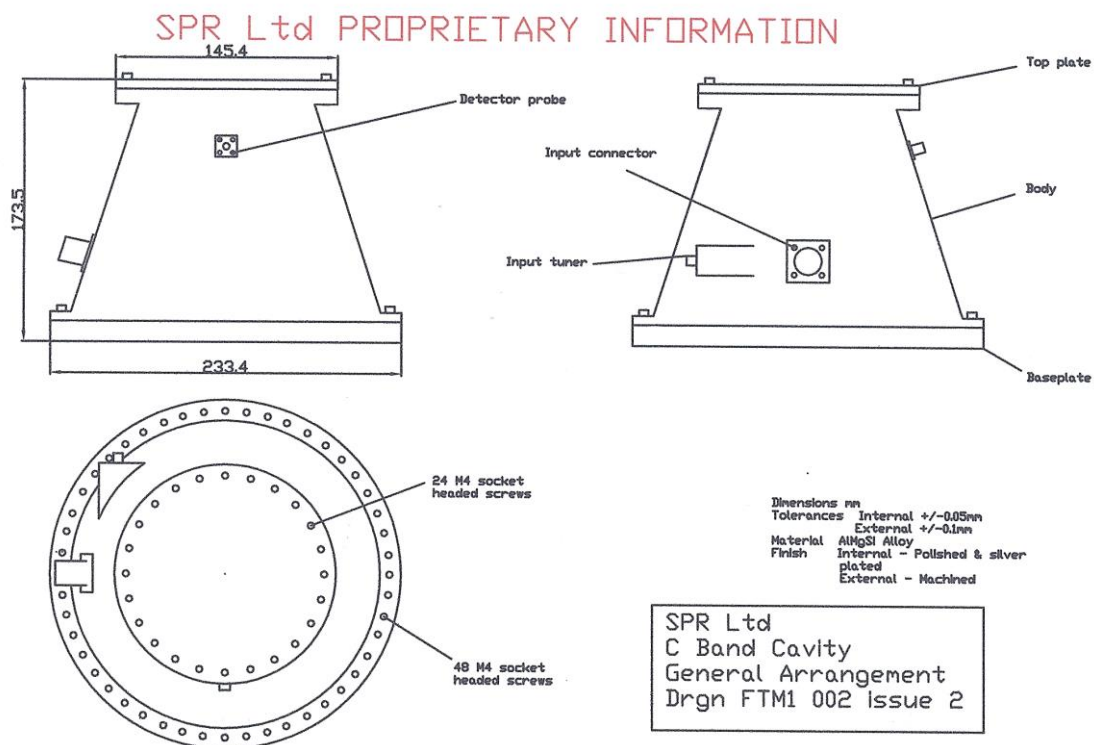


Fig 2.5 FTM General Arrangement Drawing

A major factor in achieving the required high Q value for the thruster is the wavefront distortion that can be generated by minor variation in the basic internal geometry. Clearly a simple cone with flat end plates will cause major distortion, and the actual internal shape has been developed over a number of experimental thruster programmes. The machining tolerance required to achieve the shape has also been investigated experimentally, and the results are illustrated in fig 2.6. The tolerance specified for the FTM thruster internal dimensions was +/- 0.05 mm.

Proprietary Information

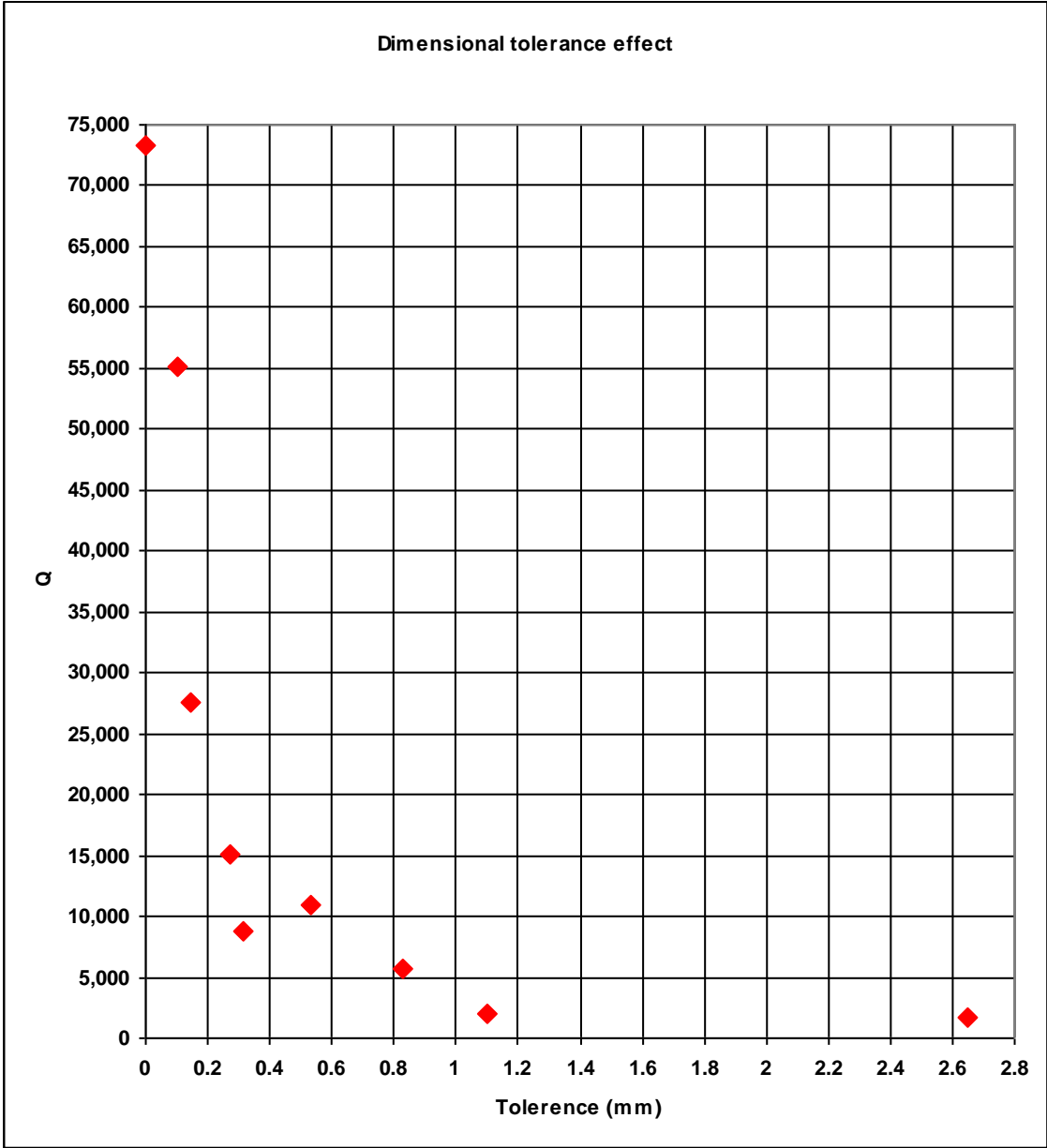


Fig 2.6 Effect of Machining Tolerance

Proprietary Information

3. Development Programme

3.1 Equipment Specification

The starting point for the development programme was “Equipment Specification for C Band Flight Thruster”, Document No. FTC03 issue A March 2007. This document was used in discussions within the space industry to establish the baseline requirements. These resulted in the following conclusions.

- a) Although the maximum power rating of the thruster is 600 W, the specified thrust will remain at 85 mN for 300 W microwave input power. This would enable operation from 2 existing flight qualified TWTAs, and enable typical technology demonstrator mission requirements to be met.
- b) The input port, identified as WGF01 in FTC03 issue A, is changed from a waveguide to a co-axial interface. This provides easier integration within the satellite.
- c) Feedback signals to the FGCU will include measurement of reflected power at the loads, and the baseplate temperature.
- d) The nominal operating frequency will be 3,850 MHz.

The equipment specification will be updated accordingly.

3.2 Flight Electrical Model (FEM)

The development programme started in October 2008, with the design of the Flight Electrical Model (FEM). The design software was updated from that used to design the Demonstrator Model, to cover operation at C Band, and to increase the axial resolution to 0.1mm.

The FEM was manufactured by fabricating the body and end plates from copper sheet, with steel supporting plates used to provide mechanical stability. The input assembly was based on a standard N type co-axial connector, with an SMA connector used for the detector probe. The FEM thruster is illustrated in Fig 3.1.

Proprietary Information



Fig 3.1 Flight Electrical Model Thruster

A simple beam balance, force measurement rig was built, enabling a programme of development tests to be carried out, with the thruster driven by a 40 Watt SSPA.

FEM development tests included:

1. Confirmation of resonant frequency
2. Measurement of loaded Q
3. Development of input circuit and tuning assembly
4. Optimisation of input and detector positions
5. Characterisation of the variation of Q with dimensional tolerance
6. Development of test bench design
7. Measurement of thrust at low input power

A total of 145 test runs were carried out with the FEM. The fabricated construction enabled connector positions to be easily varied, and different tuning assemblies to be tested. A shimming technique was developed, to enable the variation of Q with dimensional tolerance, to be fully investigated. The thrust measurements confirmed that reliable, repeatable measurements at low input power, could not be guaranteed with a co-axial cable linking the fixed source, to the suspended thruster.

3.3 Flight Test Model (FTM)

Initial development tests on the FTM, covered the effect of high power transfer in the co-axial cable link on spurious forces.

Proprietary Information

This early work resulted in a redesign of the force measurement rig to incorporate a free waveguide coupling between source and thruster. This mechanically de-couples the fixed and suspended parts of the force rig. The coupling provided a force resolution approaching the 0.1 gm resolution of the electronic balance. However, considerable design and development work was required to achieve this resolution, whilst minimising transmission loss and leakage levels.

With a stable, high-resolution test bench, the FTM underwent a long series of tests to optimise the input circuit design, and to develop frequency tracking algorithms. Frequency tracking requirements were considerably more complex than originally foreseen, due to the interaction of the thermal characteristics of the input circuit, and the cavity itself. The change in input impedance as the input circuit rapidly warms up, and the frequency effect of dimensional changes on the input loop itself, create an inherently unstable situation following initial turn on. As the cavity warms up, a second, more predictable, frequency-tracking phase dominates.

A further, important objective of the FTM development programme was to increase the loaded Q of the cavity, whilst maximising the return loss of the input circuit at resonance. This ensured that the operating point was close to the theoretical situation, where the loaded Q is half the unloaded Q, power transfer from the input circuit to the cavity is a maximum, and reflected power is a minimum.

A total of 156 development test runs were carried out. At the end of this programme, 19 further performance tests were carried out, followed by a final 2 calibration runs. The test results given in the later sections of this report are those measured during the performance and calibration tests.

4. Test Bench

4.1 Microwave Equipment

A general view of the test bench is given in Fig 4.1 where the signal generator, TWTA, circulator, cross coupler and load are shown. They are connected as illustrated in the Block diagram given in Fig 4.2.



Fig 4.1 General View of Test Bench

Proprietary Information

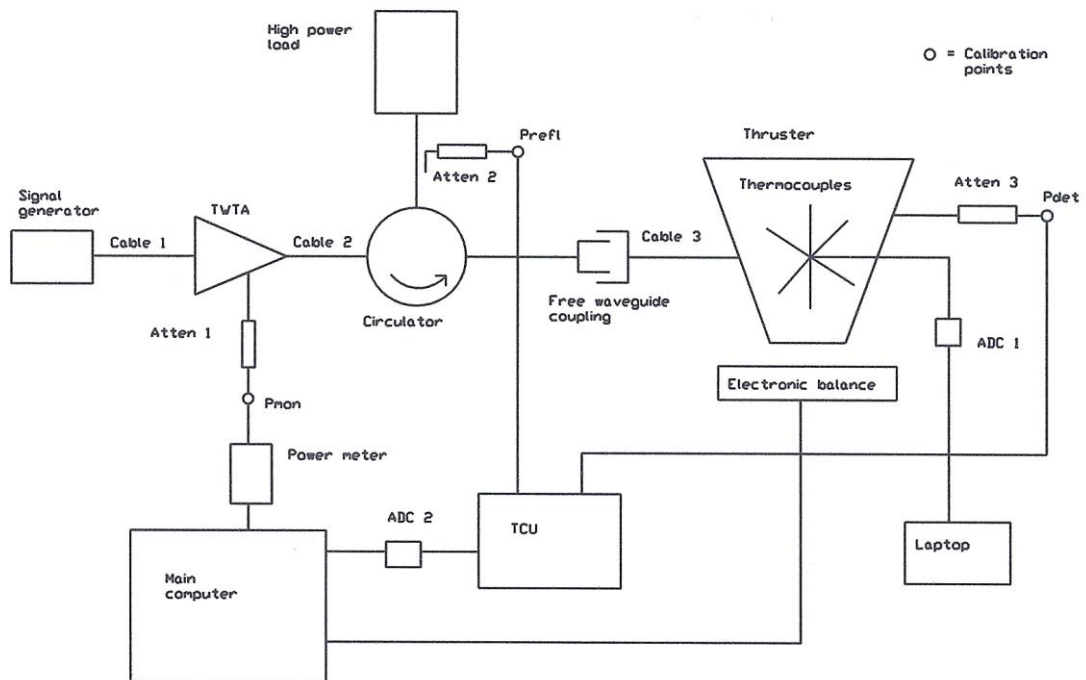


Fig 4.2 Block Diagram of Test Bench

4.2 Force Measurement Rig

The Force Measurement rig is a composite balance with the thruster suspended between an extension spring, with a spring constant of 2.8 kg/mm and an electronic balance, with a spring constant of 13.9 kg/mm. The rig is illustrated in Fig 4.3, and shown in Fig 4.4.

The spring is hung from a steel top frame, which is supported by invar rods fitted to a steel base frame. The invar rods minimise spurious force measurements, due to ambient temperature changes. The rig is mounted on a separate test bench to that supporting the TWTA, to minimise force measurement noise from the cooling fans in the TWTA, and signal generator.

The thruster itself can be mounted in two configurations, thrust vector up or thrust vector down. It is mounted between two aluminium channels, the upper channel being connected to the suspension spring.

One end of the lower channel supports a waveguide to co-axial transition, mounted on two steel rods. At the other end of the channel, a balance weight is mounted to provide adjustment of the horizontal attitude of the beam and thruster. Directly under the central axis of the thruster, a lower adjuster screw is attached to the lower channel.

Proprietary Information

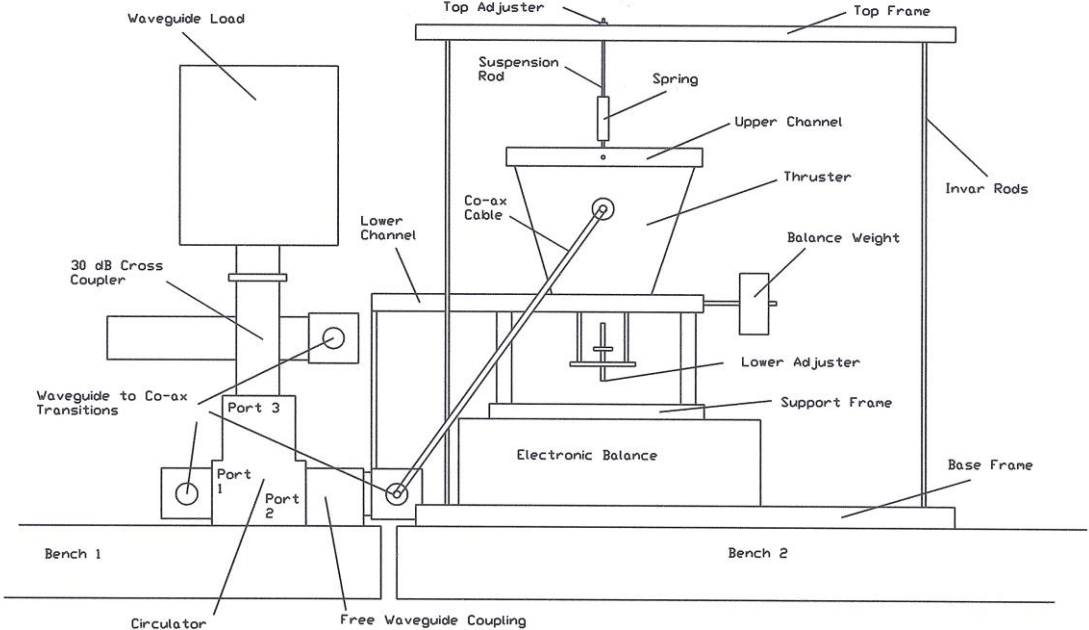


Fig 4.3 Diagram of Force Measurement Rig

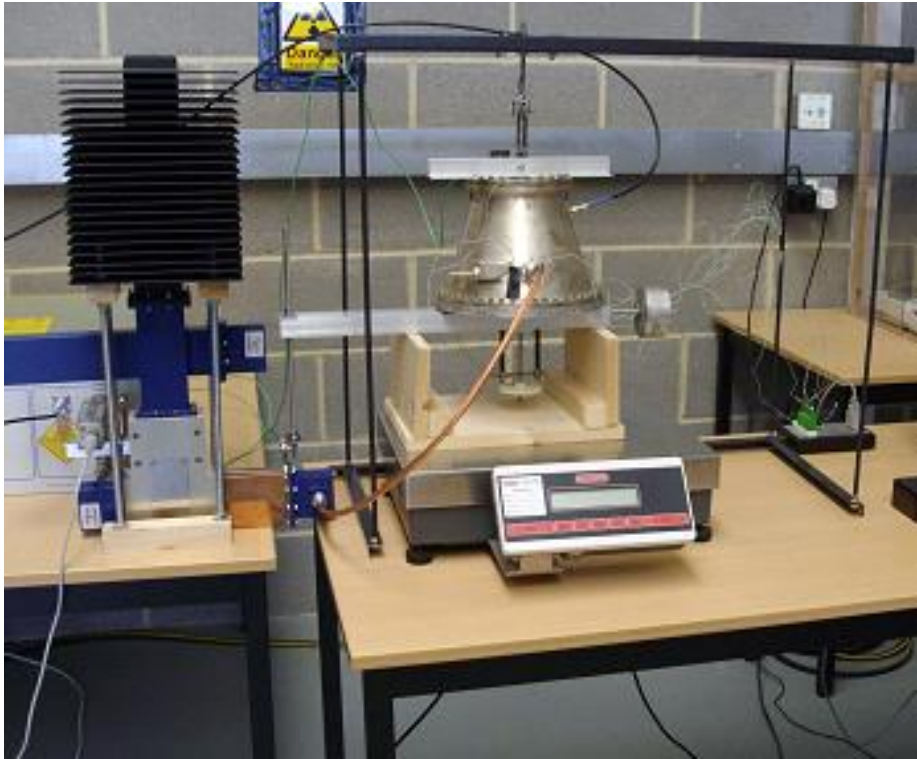


Fig 4.4 Force Measurement Rig

Proprietary Information

Spurious forces are minimised by transmitting the microwave power from port 2 of the circulator via a free waveguide coupling, where there is no mechanical coupling between the fixed and floating waveguide elements. It was found, during the development tests, that with careful mounting of a small flexible co-axial cable, it was possible to monitor detected power, during a thrust measurement test run, without producing a measurable spurious force. Similarly, the thermocouple connections, and a ground connection, could be made to the thruster, without incurring spurious forces.

The weight of the thruster can be distributed between the suspension spring and the electronic balance, by either using a screw adjuster on the top suspension rod, or by the lower adjuster, or both. During the development test programme it was found that the most stable method of adjustment, was to dispense with the lower adjustment screw, and use a wooden support frame. The pre-load (i.e. the weight supported by the electronic balance) was varied by adjusting the position of the top adjuster, whilst monitoring the electronic balance readout. Due to the high spring constant of the electronic balance, the movement of the position of the “floating” side of the free waveguide coupling was minimal, as the pre-load or the measured force changed. The microwave power to the thruster input was transmitted via a co-axial cable, whose outer sheath was removed to improve cooling. Note that the “on” period of the high power test runs was limited by the temperature rise in this co-axial cable. However as the cable is mounted between two fixed points, temperature rise and thermal expansion had no measurable effect on the force measurements.

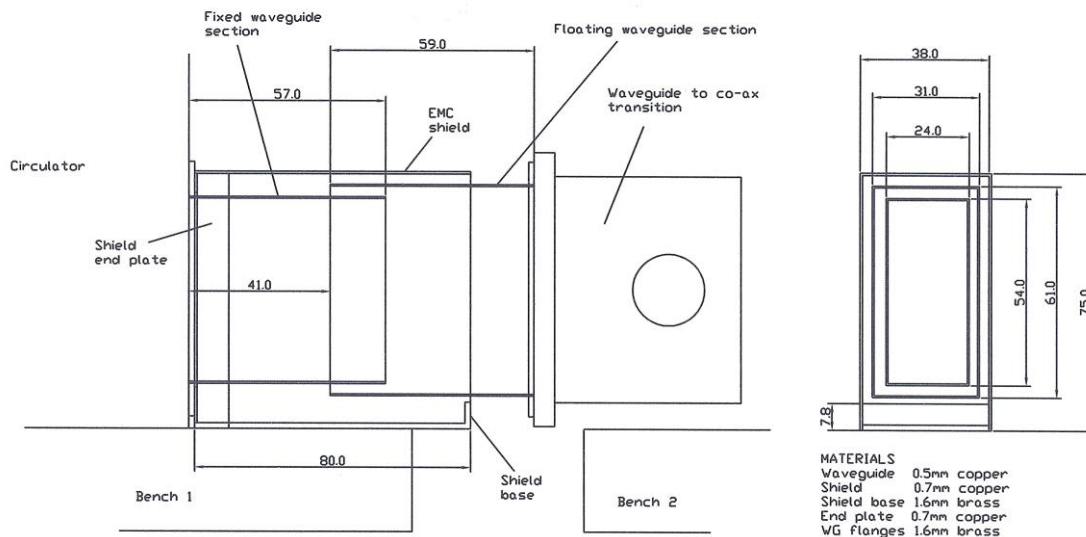


Fig 4.5 Diagram of Free Waveguide Coupling

Proprietary Information

The free waveguide coupling is illustrated in fig 4.5. The coupling consists of two waveguide sections fabricated from 0.5mm sheet copper. These are soldered into brass flanges. The fixed section is mounted on the flange fittings of port 2 of the circulator. The floating section is mounted on the flange of the waveguide to co-axial transition. The floating section is accurately aligned within the fixed section with a 3 mm gap on all sides. This gives a nominal quarter wavelength choke section whose actual length is determined by test. The length is optimised to give minimum transmission loss at the thruster operating frequency.

Leakage is minimised by surrounding the coupling with a 2 part EMC shield comprising a brass shield base and a sheet copper shield. Note that it is important that both parts of the EMC shield are bonded to the electrical ground.

4.3 Instrumentation

The digitally synthesised signal generator gave a calibrated output signal, which could be stepped in amplitude and frequency via front panel controls. TWTA output power was monitored by a digital power meter, which was connected to the main computer via a USB port. Detected power in the cavity and reflected power at the cross coupler were monitored via attenuators at ports RF1 and RF2 respectively on the Telemetry and Control Unit (TCU), originally built for the Demonstrator Engine. The TUC provides isolated and calibrated data input to the main computer via an ADC, as well as providing a digital display of both power levels. Force data is monitored at the electronic balance, via a serial link to the main computer. The electronic balance is electrically isolated, by being powered from a rechargeable battery power supply.

For EMC purposes, the thruster temperatures are monitored on a separate laptop computer, via an ADC unit. Data is transferred to the main computer via disk after each test run.

All data from a test run is recorded on an Excel spreadsheet running in the main computer. Once calibration data has been entered, the spreadsheet gives immediate graphical output for test run analysis.

Instrumentation equipment details are given in table 2.

Proprietary Information

Table 2 Test Equipment List

| Equipment | Manufacturer / Supplier | Type / Model No. |
|------------------------------|--------------------------------|-------------------------|
| Signal Generator | Agilent | 8648 D |
| TWTA | TMD Technologies | PTC 6441 |
| Circulator | Channel Microwave Corp. | A350 C |
| Power Meter | Agilent | U2001A |
| High Power load | TWS | FL-11A-HBH-202-B |
| Cross Coupler | TWS | CC-11A-AQB-202-202-B-30 |
| Waveguide / Coax transitions | TWS | RA-11A-PQB-202-B-N-F |
| Electronic Balance | Avery Berkel | FC 161 |
| Balance Power Supply | Sartorius AG | YRB 06Z |
| Thermocouples | Pico Technology Ltd | K type |
| ADC 1 | Pico Technology Ltd | TC-08 |
| Laptop Computer | HP | N5431 |
| Telemetry and Control Unit | SPR Ltd | TCU |
| ADC2 | Pico Technology Ltd | ADC-11 |
| Main Computer | Compaq | ESO79AA |
| Microwave survey meter | ETS - LINDGREN | 1501 |
| Geiger Counter | RDX Nuclear | DX-2 |
| Calibration weights | Griffin & Tatlock Ltd | 348-119 |
| Sequence Timer | RS Components | 440 – 9805 |

Proprietary Information

4.4 EMC and Safety

With high voltages present at the TWTA output, a comprehensive grounding system is used, which is checked visually before each test run. To ensure electrical noise on the telemetry data is kept to a minimum, shielded cables are used, with ground loops minimised by using a star layout. It was found necessary to completely isolate the temperature monitoring system to minimise noise, and an ambient thermocouple was used to monitor any level change during “on” periods.

Calibration procedures included EMC checks, at full power, to eliminate any EMC errors in the measured data.

The free waveguide coupling was a source of considerable signal leakage during high power runs. The leakage field at the operator position was continuously monitored, to ensure a safety level of 5 mW/cm² was not exceeded.

A hand held Geiger counter was also used to check for possible X-ray emission, although no emissions were detected during the test programme.

5. Test Procedures

5.1 Tuning and Q measurement

Tuning the cavity for maximum loaded Q was a lengthy, iterative process and occupied much of the development test programme. Quick Q measurements were taken, by offsetting the input frequency from the resonant value, until detected power was halved, and then calculating the 3 dB bandwidth. This then gave the loaded Q, at the resonant frequency.

Once the desired tuning point had been achieved, a plot of the detected power and reflected power against input frequency was taken, by stepping the frequency over the required range. For accurate Q determination, this was carried out for both increasing and decreasing frequency steps, with a mean plot calculated. At least 100 steps were used per plot. A typical plot is given in fig 5.1.

The first step in the tuning process was to determine the optimum input loop dimensions, for an untuned input circuit. A series of different loops were manufactured, and Q measurements were made to optimise maximum Q, whilst maintaining a minimum offset, from the basic cavity resonant frequency. Although detected power was primarily used in this process, in later stages, the detector was replaced with a tuning screw and the Q maximised, using the reflected power characteristic.

As the loop dimensions approached optimum, the second step was to use the input tuning screw to minimise the value of the reflected null, and increase the

Proprietary Information

value of the detected peak. A clear indication of when optimum loop dimensions were achieved, was a set of symmetrical peak and null plots, as shown in fig 5.1. Asymmetry in these plots indicated that input circuit and cavity resonant points were not correctly aligned.

A further consideration in the loop dimensions, was the need to decrease electrical loss in the loop itself, due to the very high currents flowing at resonance. The cross section of the loop conductor underwent a number of development cycles to minimise loss, and to enable stable frequency tracking algorithms to be developed, for different input power levels.

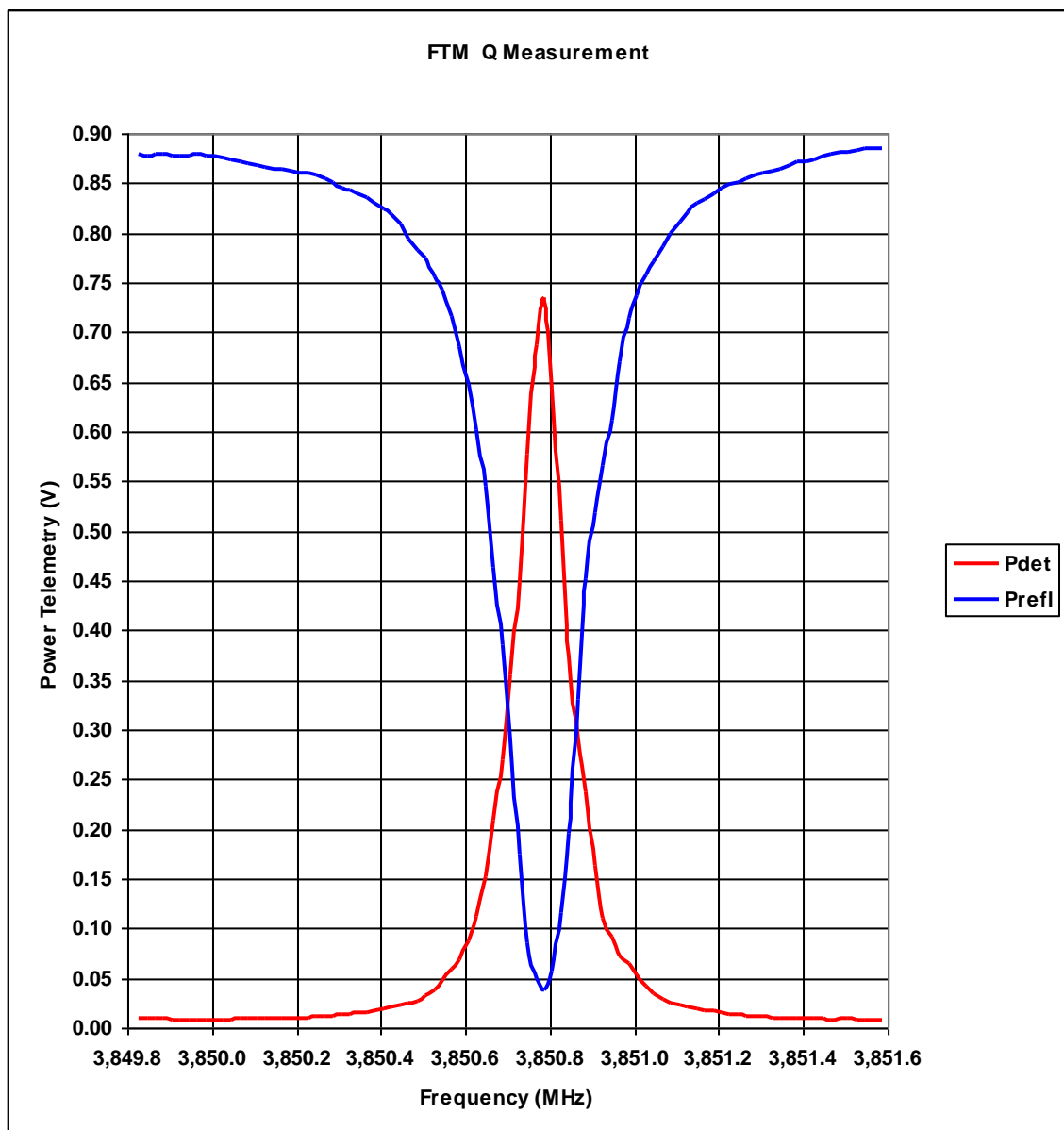


Fig 5.1 FTM Resonant Frequency Plot

Proprietary Information

5.2 Power measurement and calibration

The digital power meter, normally connected to the TWTA output power monitor, was used in routine calibration of the cables and microwave equipment shown in fig 4.2. The main calibration points are shown as:

| | | |
|-------|---|---------------------------------|
| Pmon | - | TWTA output power |
| Pdet | - | Cavity detector power telemetry |
| Prefl | - | Reflected power telemetry |

Typical calibration data is given in figs 5.2 and 5.3. The gains and losses for microwave cables and equipment are given in table 3, together with typical power levels for a high power run. Note that the main variable was the TWTA gain, which necessitated recording of the TWTA power output, at Pmon, for each test run.

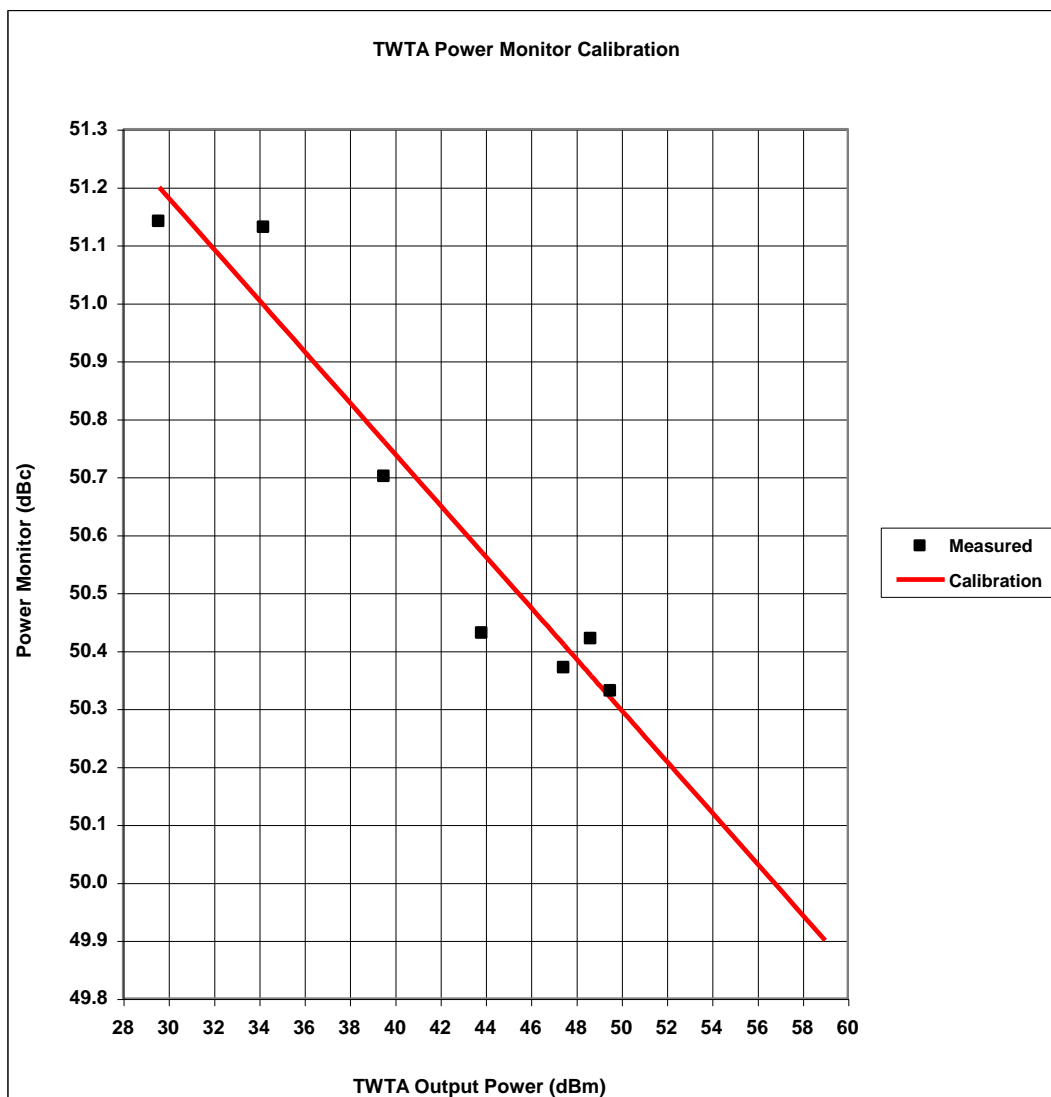


Fig 5.2 Pmon Calibration

Proprietary Information

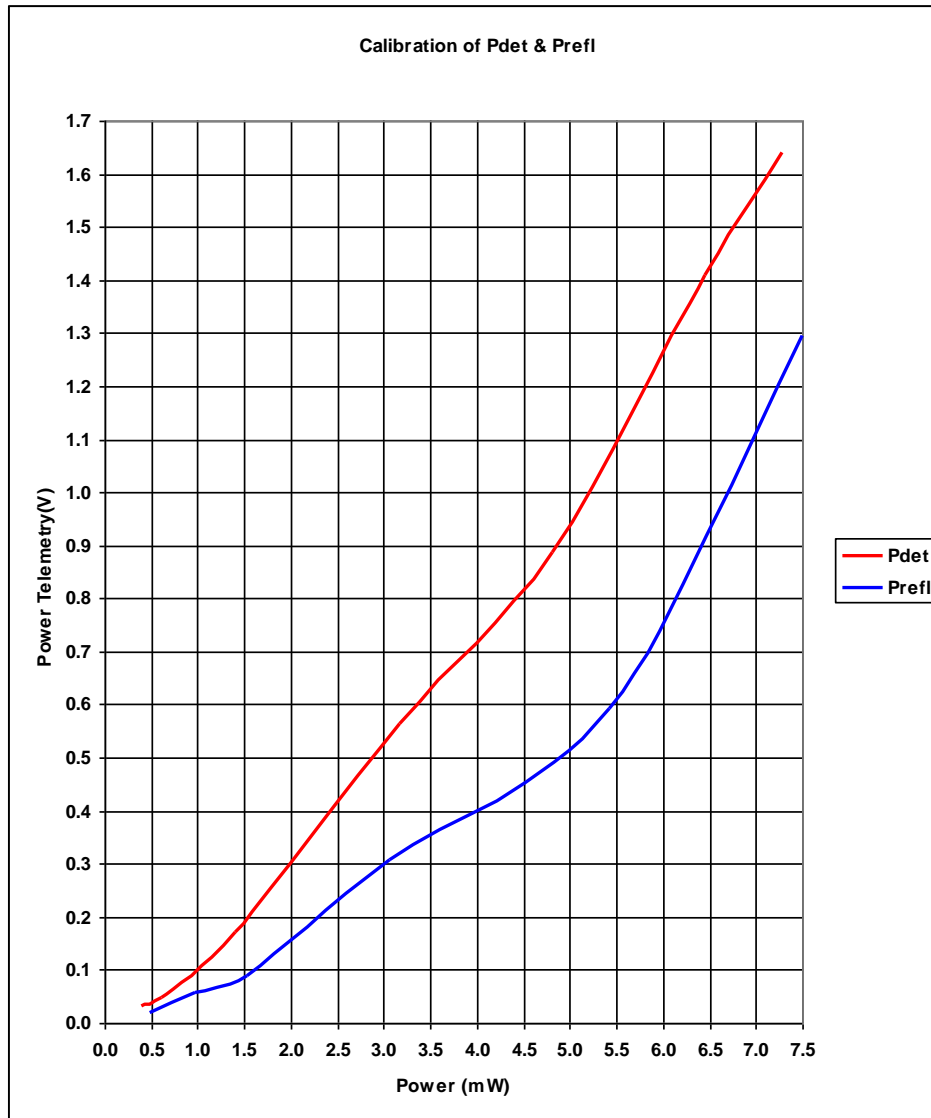


Fig 5.3 Pdet and Prefl Calibration

| Equipment | Gain / Loss (dB) | Ouput Power (W) |
|------------------------------|------------------|-----------------|
| Signal Generator | | .00016 |
| Cable 1 | -2.18 | .0001 |
| TWTA | 68.1 | 619.4 |
| Cable 2 | -0.13 | 601.2 |
| Circulator (forward) | -0.15 | 580.8 |
| Waveguide Coupling (forward) | -0.26 | 547 |
| Cable 3 | -0.51 | 486.4 |
| Thruster return loss | -9.16 | 59 |
| Waveguide Coupling (reverse) | -0.57 | 46 |
| Circulator (reverse) | -0.08 | 45.2 |
| Cross Coupler | -30 | 0.045 |

Table 3. Microwave Power Levels and Losses

Proprietary Information

5.3 Frequency Tracking

The later development tests were primarily aimed at establishing frequency tracking algorithms, for test runs at 3 nominal input power levels.

| | |
|--------------------|-------|
| Low power tests | 150 W |
| Medium power tests | 300 W |
| High power tests | 450 W |

These correspond to possible flight engine configurations using one, two or three existing flight qualified TWTAs.

Frequency tracking algorithms were necessary, because at initial power turn on, the input loop rapidly increases in temperature, due to high currents at resonance. This results in small dimensional changes, and hence a shift in resonant frequency. The feedback effect of frequency shift, gives an inherently unstable circuit at turn on, and also at any point in the test run when resonance is lost.

This effect is countered by determining a frequency offset, to be applied at power turn on, followed by a stepped frequency increase during the following phase of input circuit warm up. The rate of frequency increase is determined by monitoring the reflected power telemetry at the TCU. The level is maintained above a critical level to avoid loss of resonance.

Once the input circuit has reached a stable temperature, with the input frequency at resonance, the effect of the wall temperature increase comes into prominence. The temperature increase results in an effective increase in cavity length, and it becomes necessary to progressively reduce the input frequency, to maintain resonance. Once again, reflected power is monitored at the TCU, and the rate of frequency decrease is varied to keep P_{refl} above the critical level. Fig 5.4 gives a typical frequency tracking result for a medium power test run.

Proprietary Information

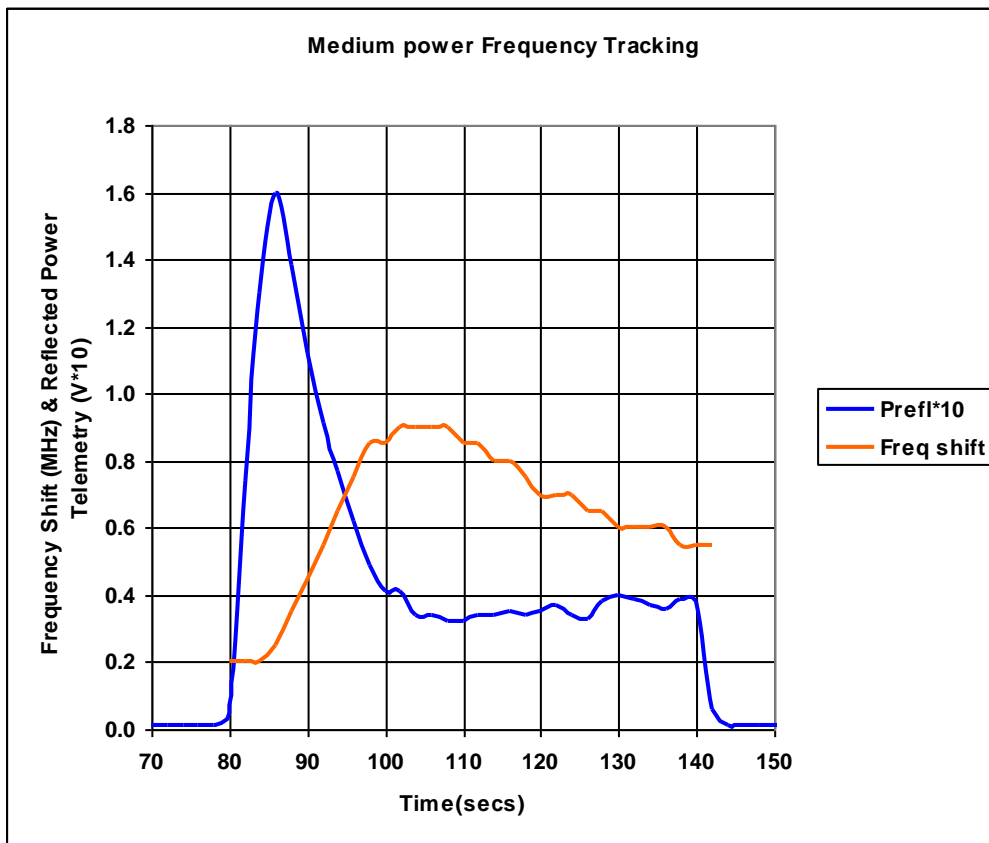


Fig 5.4 Frequency Track for Medium Power Run

For this test run (FTM 169), the initial frequency offset was 0.2MHz. After 6 seconds from power on, the frequency was increased for 14 steps of .05MHz at approximately one step per second. This was followed by a 7 second period at constant frequency, then by a frequency decrease of 7 steps, at one step approximately every 4 seconds. The minimum reflected power telemetry was set to .03V. Table 4 gives typical tracking algorithms for the three nominal power levels

| Nominal Input Power | Low | Medium | High |
|-----------------------------------|-------|--------|------|
| Freq offset (MHz) | 0.05 | 0.2 | 0.25 |
| Freq step (MHz) | 0.025 | 0.05 | 0.05 |
| Rate of Freq increase (secs/step) | 2 | 1 | 1 |
| No. of Freq increase steps | 6 | 14 | 20 |
| Period of constant Freq (steps) | 15 | 7 | 6 |
| Rate of Freq decrease (secs/step) | 5 | 4 | 4 |
| No of Freq decrease steps | 9 | 7 | 5 |
| On period (secs) | 90 | 60 | 60 |
| Minimum Prefl. (v) | .005 | .03 | .07 |

Table 4. Frequency Tracking Algorithms

Proprietary Information

For a flight qualified engine, the algorithms would be determined by characterising each flight thruster, and mapping the data into the control processor of the FGCU. Feedback data of detected power, reflected power and baseplate temperature would be used to control the input frequency, over the full qualification temperature range, for the required input power range.

5.4 Force Measurement and Calibration

Force Measurement Principles

The force measurement rig is designed to measure the Reaction Force (R) rather than the Thrust (T) produced by the thruster. The difference between the two forces is best illustrated by assuming the thruster is in free space, as illustrated in fig 5.5.

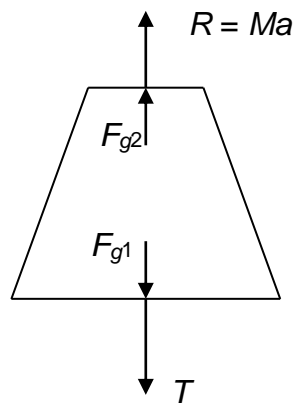


Fig 5.5 Thruster Force Diagram

The net force (F) created within the thruster is given by the basic equation

$$F = Q(F_{g1} - F_{g2})$$

where F_{g1} and F_{g2} are the radiation forces caused by group velocities V_{g1} and V_{g2} at the two ends of the thruster.

This internal force F is measured by an outside observer as the Thrust T , a force acting against the observer in the direction shown.

Newton's laws state that T must be opposed by an equal and opposite reaction force R , such that

$$R = Ma$$

where M = mass of the thruster

a = acceleration of the thruster in the direction shown.

Proprietary Information

Clearly, where T and R exist, they will cancel out any attempt to measure them by simply placing the thruster on a balance. This is demonstrated by the results of the calibration test shown in Fig.5.9.

The force measurement rig is designed to measure the Reaction force dynamically, by measuring the change of acceleration of the centre of mass of the thruster, caused by the Reaction force.

During a test run, because there is no thermal compensation in the flight thruster design, the walls of the thruster will expand. The large difference in spring constants of the suspension spring and the electronic balance, mean this wall expansion will cause the centre of mass of the thruster to move. The movement is recorded as an increase in the pre-load, measured on the electronic balance. The acceleration in this movement, caused by the Reaction force, is measured as an increase or decrease in the pre-load depending on the attitude of the thruster. Thus with the thrust vector down, (as illustrated in fig 5.5), the Reaction force is up, and the pre-load increase will be slightly decreased.

The effect is illustrated in the test run simulation results given in fig 5.6. A plot of actual temperature rise is given, whilst up and down force measurements are simulated to show the effect on a single chart. The reference slope is also shown, which enables the reaction force plots to be calculated. For actual test runs, the reference slope is taken to be a straight line between the start and stop timings of the recorded test data. The reference timings account for some of the test data scatter, as the timing resolution is +/-2 secs. The linear reference slope can be seen to be a good approximation, from the linearity of the temperature data in fig 5.6.

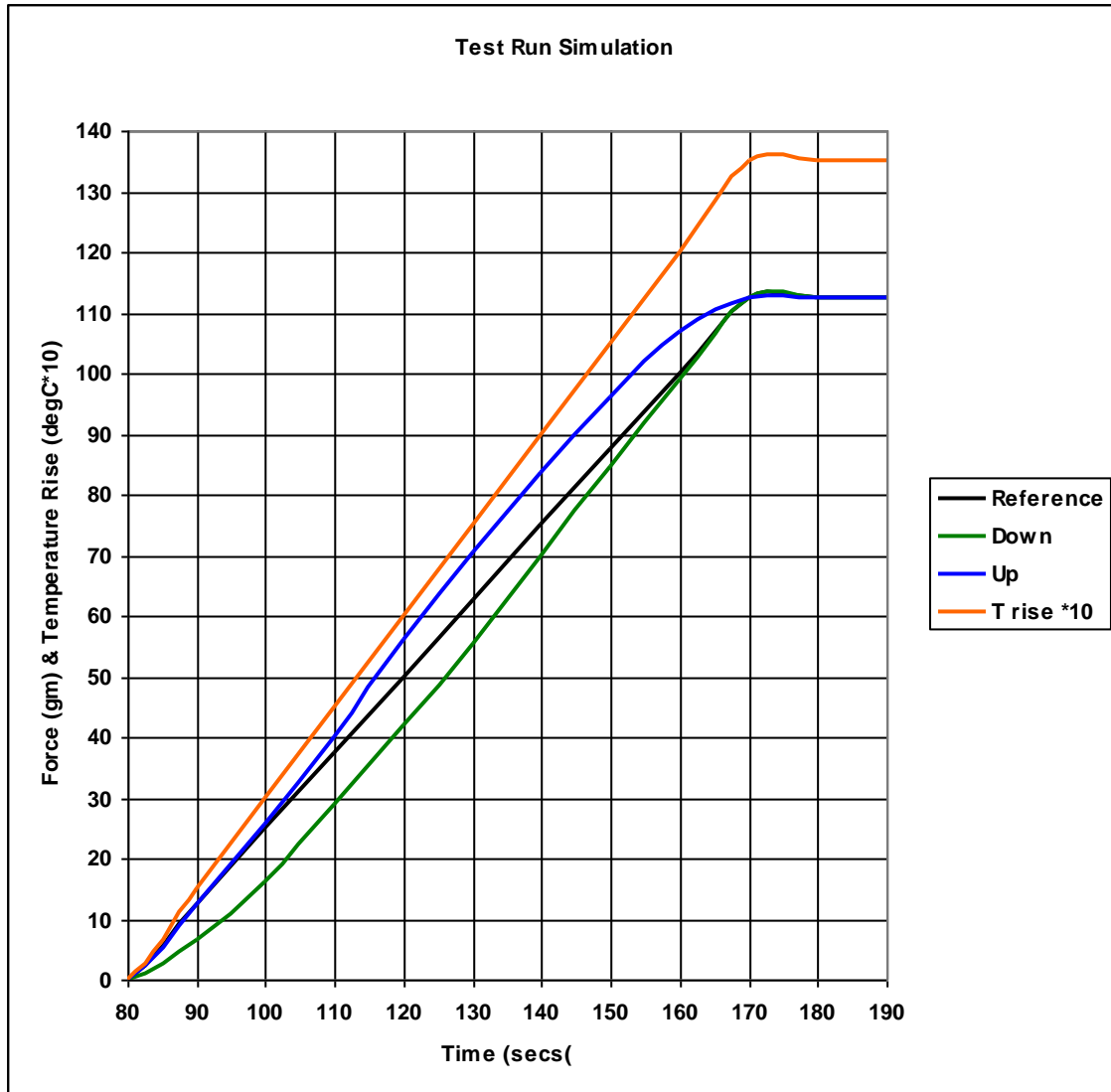


Fig 5.6 Simulation of Test Runs

Rig Calibration

The first step in calibrating the force measurement rig, was to carry out force / extension measurements on both the spring suspension assembly and the electronic balance. The two actual spring constant plots are given in fig 5.7 This data was then used to produce a simple mathematical model of the force measurement rig. This predicted reasonably linear operation from 1.5 kg to 6 kg pre-load.

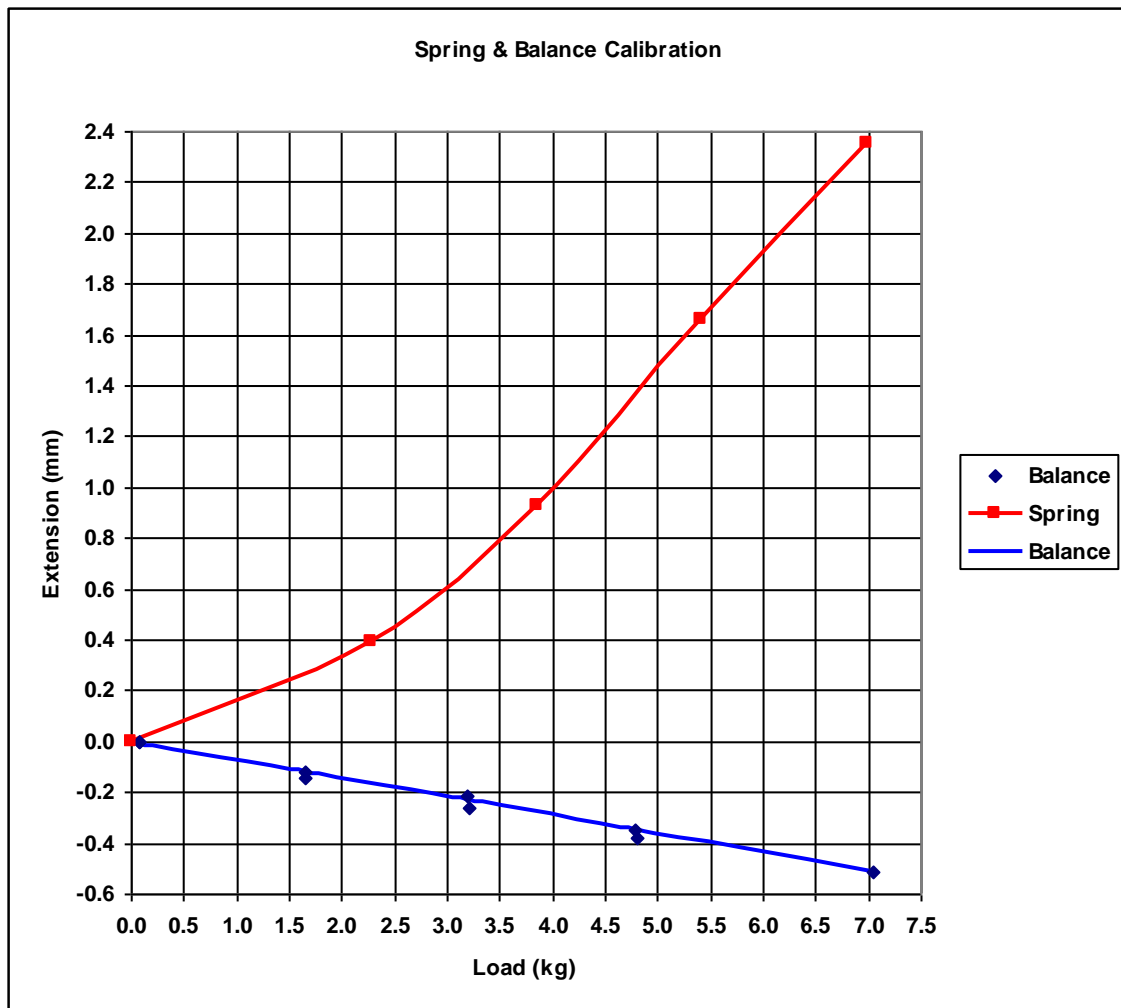


Fig 5.7 Spring and Balance Calibrations

A calibration characteristic for the test rig was measured, by starting with a zero pre-load. This condition was when the suspension spring was taking the full weight of the thruster, and the electronic balance was registering zero. From this point, pre-load was introduced by applying rig compression by adjusting the top screw adjuster, and thus increasing the length of the suspension rod. The resulting calibration characteristic is shown in fig 5.8 together with the model prediction.

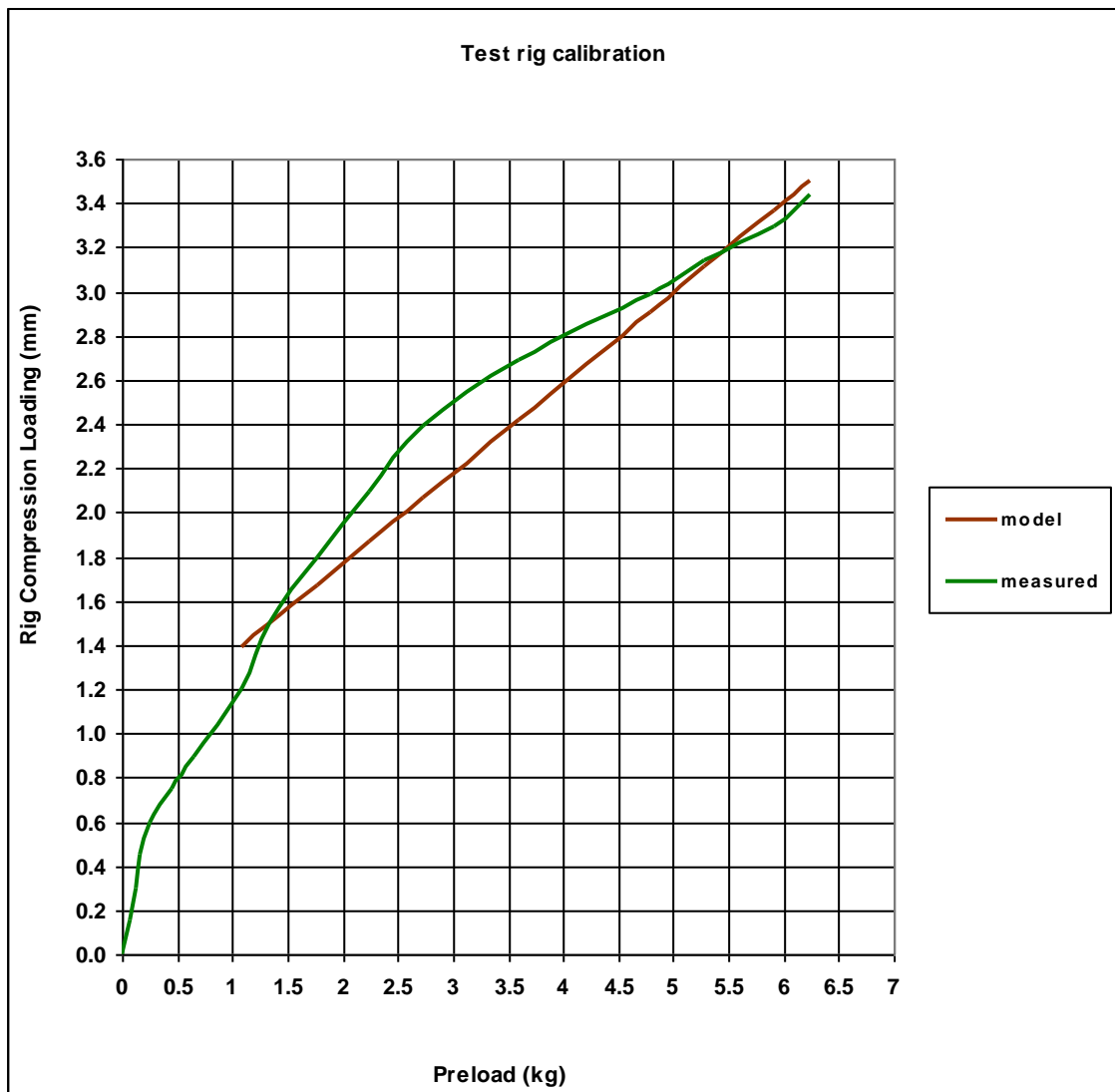


Fig 5.8 Force Measurement Rig Calibration

The performance test runs were carried out with two pre-load settings of 2 kg and 5 kg. No discernible effect on the test data was noted from the different pre-load settings.

Finally, each set of test runs was preceded by a simple calibration routine. This consisted of applying a 10 gm weight to the thruster and removing it. This was repeated a number of times, and the calibration factor was calculated from the measured change of pre-load. A mean calibration factor from all the calibration checks was calculated as 0.86. This compares well with the calibration factor of 0.82, determined from the mathematical model.

Proprietary Information

To determine the effect of spurious forces generated during test runs, a pair of calibration runs, test numbers FTM 176 and FTM 177, were carried out at the end of the performance test programme.

These calibration test runs were carried out with the electronic balance carrying the full weight of the thruster, and therefore no increase in pre-load, due to thermal expansion or Reaction force, was measured. The only force data recorded by the balance, was due to spurious forces, EMC effects, or the resolution of the balance itself. Test FTM 176 was with the thrust vector up, and Test FTM 177 was with the thrust vector down. Both tests were carried out at medium input power. The results of Test FTM 177 are given in fig 5.9. The mean spurious force measured over both runs was -0.102 gm with a standard deviation of 0.192 gm. Note that the measurement resolution of the electronic balance is ± 0.1 gm.

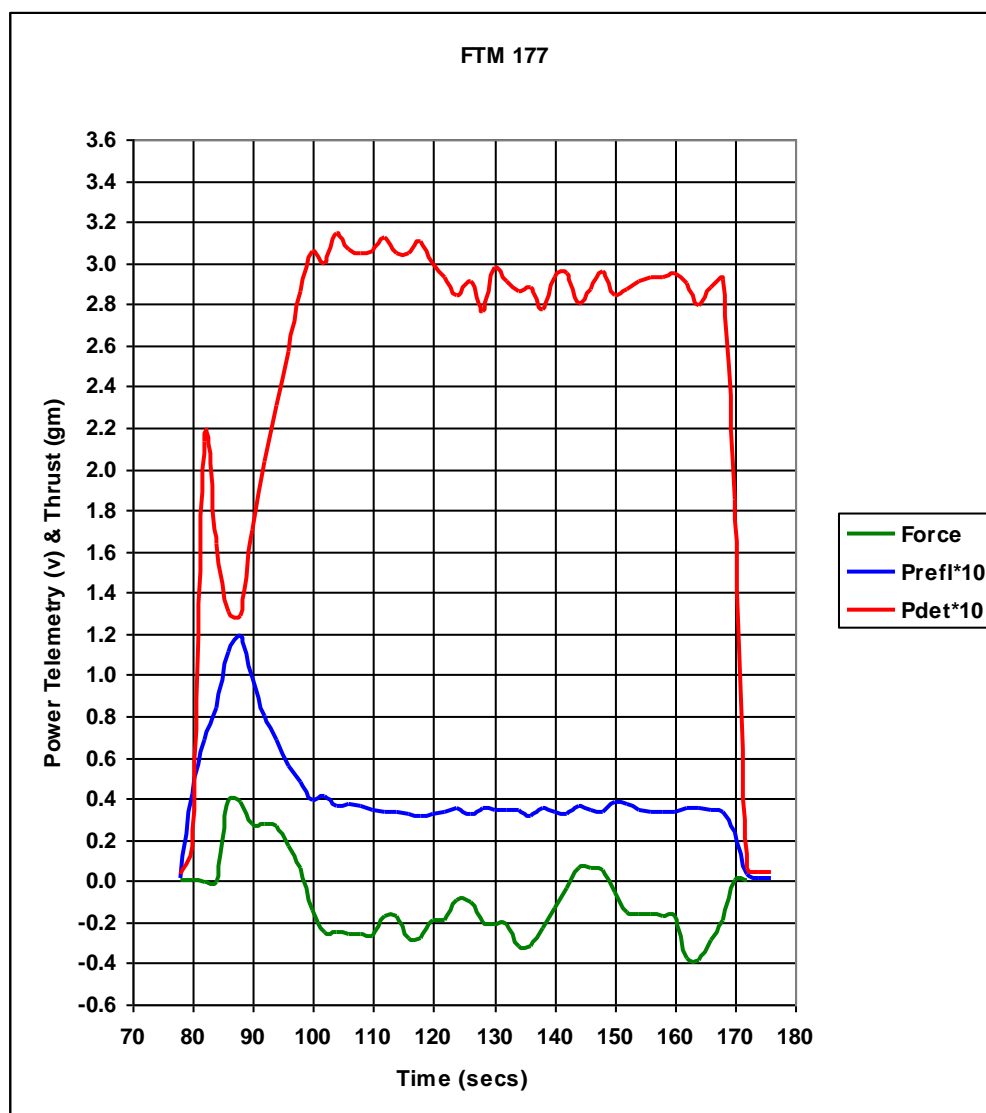


Fig 5.9 Test FTM177 Spurious Force

Proprietary Information

Test Run Procedure

Test runs, carried out during the development and performance test programmes, were designed to produce the following data:

- Reaction Force
- TWTA output power
- Cavity detected power
- Cross coupler reflected power
- Input frequency
- Temperature data at 6 points on the thruster

All data except the TWTA output power and Input Frequency were recorded at 2 sec intervals on the main computer. TWTA output power was noted with spot measurements throughout the run, and was seen to be constant. Frequency data was taken at each frequency step of the tracking algorithm.

The development test runs were carried out in a 200 sec sequence, with “Power on” periods of 30 secs, 60 secs or 90 secs. The first 15 performance tests were carried out with “Power on” periods of 90 secs, and the last 4 performance tests with a 60 secs “Power on” period, (see section 5.5).

Immediately prior to starting the test run sequence, the resonant frequency was determined. Attenuator 2 was set to – 6dB, and the signal generator output amplitude set to – 30 dBm. Resonance was found by searching for a null, using the Prefl readout on the TCU. Attenuator 3 was left at 26dB. The nominal input power at the thruster for this measurement was 4 W.

Attenuator 2 was then increased to 26 dB, and the signal generator amplitude set to

- 15 dB lower power runs
- 11 dB medium power runs
- 9dB high power runs

Note that the TWTA gain variation gave a scatter of actual thruster input powers, around the nominal 150 W, 300 W or 450 W. However the key performance figure for the thruster is the Specific Thrust in mN/kW, over the full, specified power range.

Proprietary Information

The Test Sequence was as follows:

| <u>Time (secs)</u> | <u>Operation</u> |
|--------------------|-----------------------------|
| 0 | Sequence timer on |
| 10 | Temperature recorder on |
| 20 | Power recorder on |
| 30 | Balance recorder on |
| 90 | Power on |
| 120/ 150 /180 | Power off |
| 200 | All telemetry recorders off |

5.5 Temperature Measurement

Six thermocouples were available for temperature monitoring, and were deployed as follows:

| | |
|----|----------------------------------|
| T1 | Thruster baseplate |
| T2 | Thruster top plate |
| T3 | Thruster input |
| T4 | Thruster wall |
| T5 | Free Waveguide Coupler / Ambient |
| T6 | Thruster detector/ cable 3 |

T1 to T4 were maintained in the same position throughout the test programme. T5 was initially positioned on the static section of the Free Waveguide Coupler. This was to monitor for any change in loss in this component. Once it had been established that the loss was constant, the thermocouple was repositioned to monitor ambient temperature. This enabled any correction to the temperature data, due to residual EMC effects, to be determined. The maximum correction required was 1.5 deg C.

T6 was initially positioned close to the Thruster detector, to monitor for any change in detector losses, but as these remained undetectable, the thermocouple was repositioned on the input cable, (cable 3), after a failure of this cable. The cable losses were causing very high temperature increases during high power runs. For a 90 sec, medium power run, the temperature increased by 33 deg C. Following the replacement of the cable, subsequent test runs were restricted to 60 sec "power on" periods.

Proprietary Information

6. Test Results

6.1 Specific Thrust

The main performance parameter of an EmDrive Thruster is the Specific Thrust. The results of the 19 performance tests, which characterised the specific thrust over the nominal input power range of 150 W to 450 W, are given in table 5.

| FTM test number | Thrust vector | Input power | Pfwd (Watts) | Prfl (Watts) | Pin (Watts) | Thrust (gm) | Sp thrust (mN/kW) |
|-----------------|---------------|-------------|--------------|--------------|-------------|-------------|-------------------|
| 142 | up | medium | 292 | 23 | 269 | 10.6 | 386 |
| 143 | up | medium | 297 | 24 | 273 | 12.3 | 442 |
| 144 | down | medium | 348 | 19 | 329 | -8.2 | 244 |
| 145 | down | medium | 360 | 13 | 347 | -11.6 | 327 |
| 153 | up | medium | 366 | 20 | 346 | 10.1 | 287 |
| 154 | up | medium | 361 | 25 | 336 | 13.1 | 383 |
| 155 | up | low | 173 | 13 | 160 | 4.5 | 275 |
| 156 | up | low | 144 | 14 | 130 | 4.3 | 326 |
| 157 | up | high | 427 | 71 | 356 | 12.6 | 348 |
| 159 | up | high | 456 | 59 | 397 | 14.2 | 350 |
| 160 | up | high | 486 | 59 | 427 | 17.7 | 405 |
| 162 | up | high | 482 | 59 | 423 | 15.7 | 365 |
| 163 | down | low | 172 | 12 | 160 | -3.5 | 215 |
| 165 | down | high | 485 | 28 | 457 | -17.0 | 364 |
| 167 | down | low | 162 | 6 | 156 | -3.2 | 201 |
| 168 | down | medium | 359 | 17 | 342 | -8.4 | 241 |
| 169 | down | medium | 356 | 32 | 324 | -9.2 | 278 |
| 174 | down | high | 416 | 69 | 347 | -12.5 | 353 |
| 175 | down | high | 395 | 68 | 327 | -13.5 | 403 |

Table 5. Performance Test Results

The mean specific thrust for the 19 tests was calculated as 326 mN/kW, with a Standard Deviation of 67 mN/kW.

The mean specific thrust for tests with the Thrust Vector up, was 357 mN/kW.

The mean specific thrust for tests with the Thrust Vector down, was 292 mN/kW.

The forward power (Pfwd), given in table 5, is calculated from the calibrated power monitor on the TWTA output, and the measured losses up to the Thruster input.

Proprietary Information

The reflected power, given in table 5, is calculated at the Thruster input, from the calibrated telemetry Prefl, and the measured losses to the cross coupler output.

The input power to the thruster (p_{in}), is the difference between the forward and reflected powers.

The scatter in the specific thrust data is illustrated in fig 6.1, where thrust is plotted against input power.

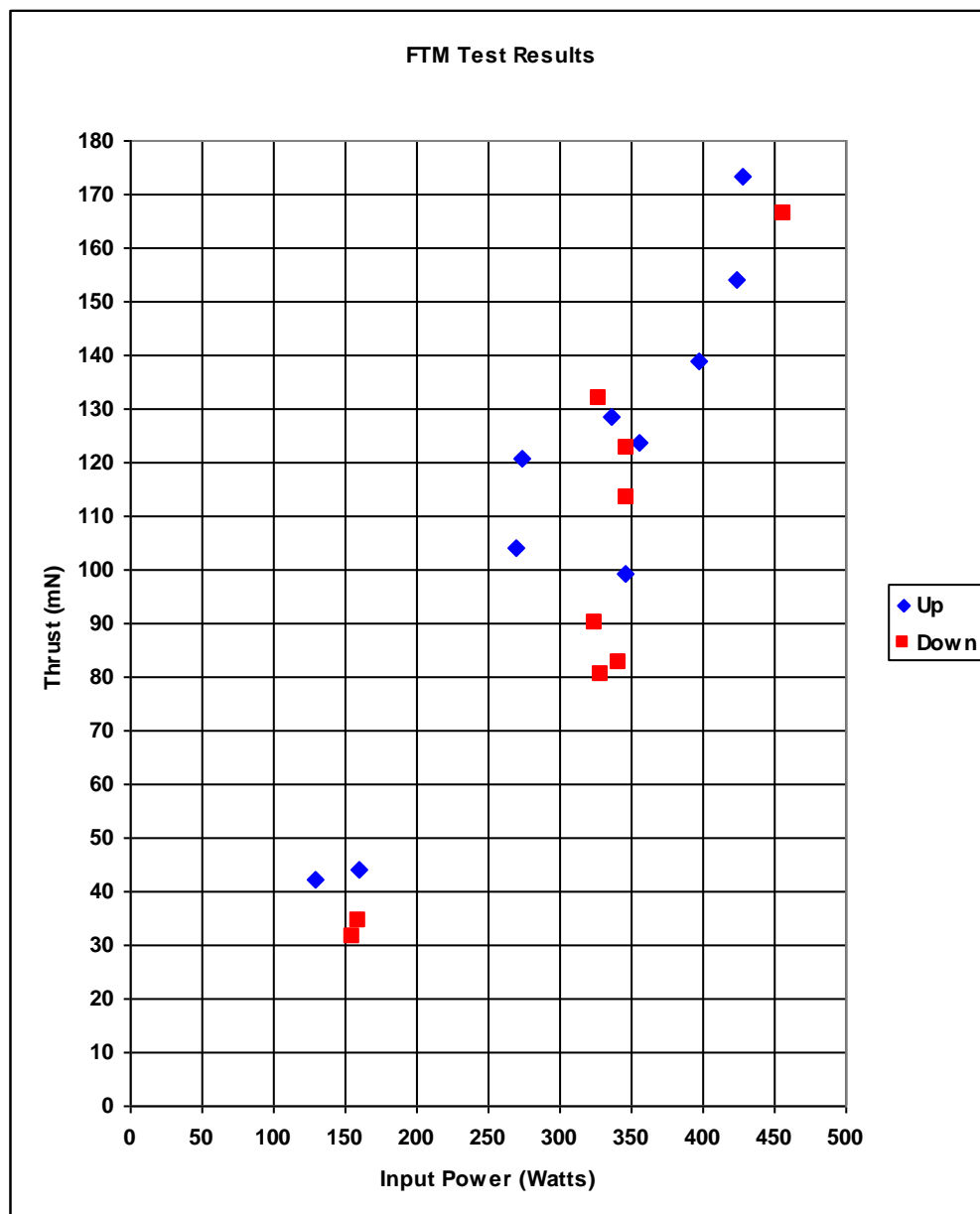


Fig 6.1 Thrust Data for Performance Tests

Proprietary Information

6.2 Reaction Force plots and analysis

The reaction force for a typical test run is given in fig 6.2. Test FTM 169 was a medium power run, with the Thruster mounted with the thrust vector up. This gives a reaction force down and hence an increase in pre-load reading on the balance.

The reaction force plot is therefore positive when the reference slope is subtracted from the electronic balance data. (See Section 5.4.1 and fig 5.5.)

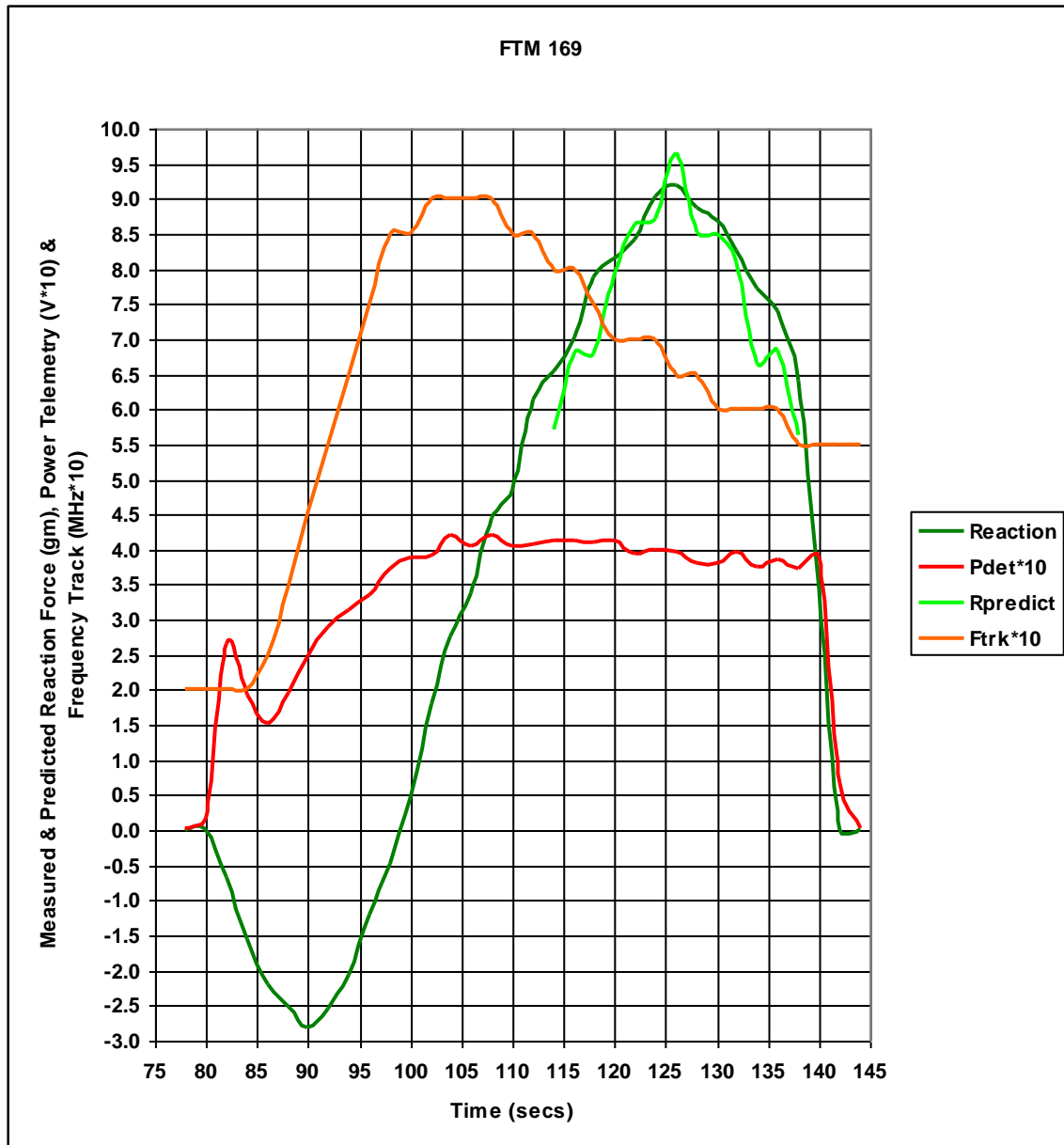


Fig 6.2 FTM 169 Test Results

Proprietary Information

Fig 6.2 shows that the Reaction force follows a positive peaked curve once the Pdet plot reaches a constant at around 100 secs. At this point, the frequency plot reaches a maximum, showing the input loop temperature has reached a stable value. From this point in the run, until power off at 140 secs, the frequency is stepped down to compensate for the increasing cavity length as the wall temperature increases.

The reason why the Reaction force plot is a peaked curve, whilst the Pdet plot is constant, is because Thrust, and hence Reaction Force, is proportional to the unloaded Q of the cavity, whilst the detected E field is proportional to the loaded Q.

The equivalent circuit of the thruster can be considered as two resonant circuits in series, one an external circuit consisting of the input and the detector, and one the cavity itself. Circuit theory states that when the impedances of the two circuits match, power transfer will be a maximum, and reflected power a minimum. This is the situation at the peak of the Reaction Force plot, when the input frequency matches the resonant frequency of the thruster. At this point, the Q of the two circuits will both be equal to the unloaded Q of the cavity (Q_u). The Q, as seen at the input of the thruster, will however be the loaded Q, (Q_l) which will be half Q_u .

Q_l and Q_u are illustrated by Pdet / frequency plots in fig 6.3. The difference between Q_l and Q_u is shown in fig 6.4. This difference, when scaled for a maximum of 1.0 is the ratio of Thrust to Pdet .

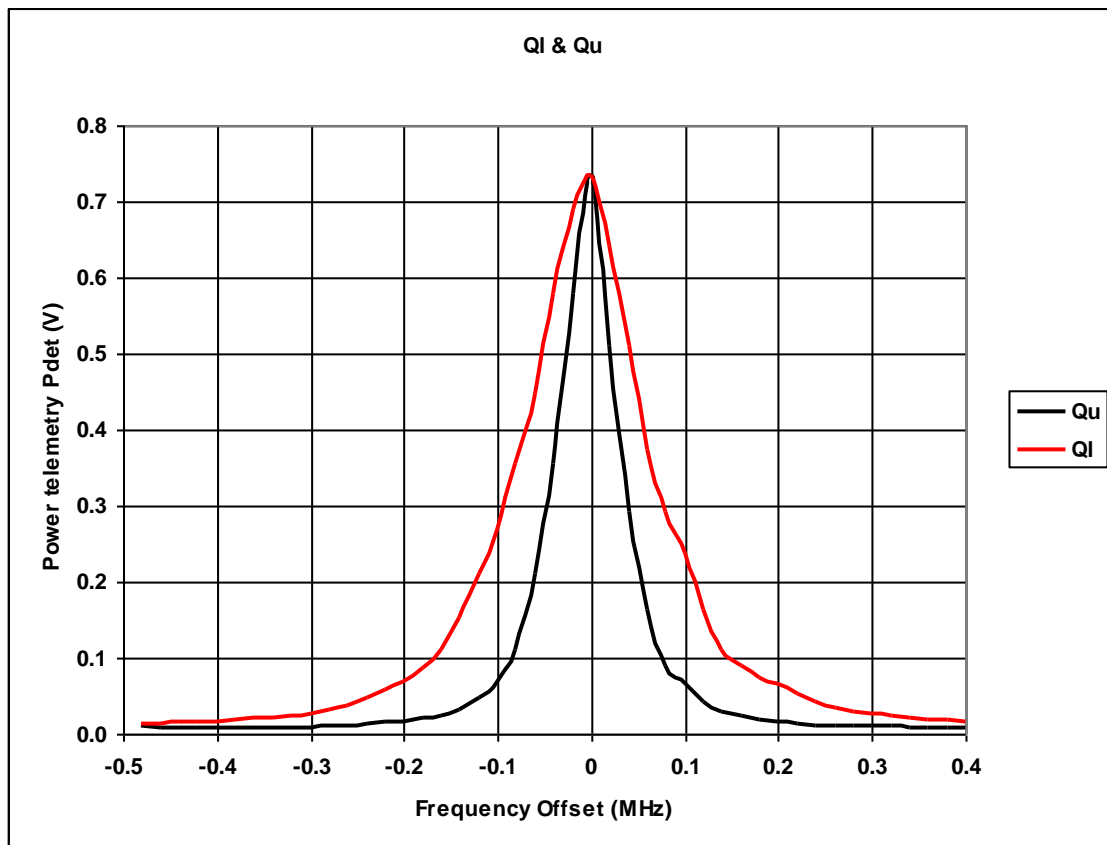


Fig 6.3 Loaded and Unloaded Q

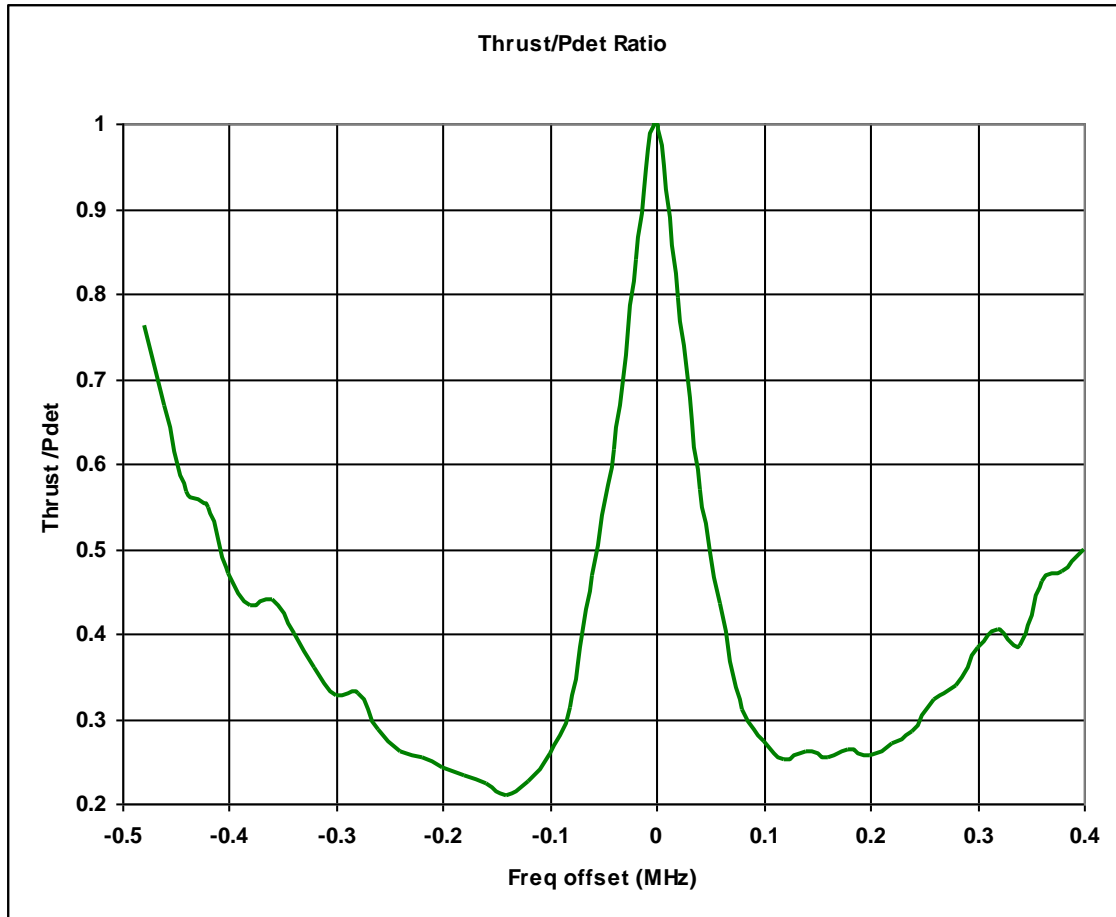


Fig 6.4 Thrust / Pdet ratio Plot

The Reaction Force, either side of resonance, was predicted for test FTM 169 using

- (a) The measured input power
- (b) The mean specific thrust for “up” tests
- (c) The measured wall temperature
- (d) The ambient temperature
- (e) The measured temperature coefficient (see Section 6.4)
- (f) Fig 6.4

The predicted Reaction Force ($R_{predict}$) shown in fig 6.2 is in good agreement with the actual measured force around resonance.

6.3 Resonant Frequency Tracking Results

The effects of frequency tracking during test runs are illustrated by comparing the results of tests FTM 157 and FTM 174.

Test FTM 157 was a high power test, with the thrust vector down, and a “power on” period of 90 secs. Approximately 50 secs into the “power on”

Proprietary Information

period, resonance was lost, as the cavity thermal expansion was not compensated soon enough, by frequency tracking.

Test FTM 174 was a high power test with a “power on” period of 60 secs, and the thrust vector up. Resonance was maintained throughout the run by compensating the cavity thermal expansion, with early negative frequency tracking.

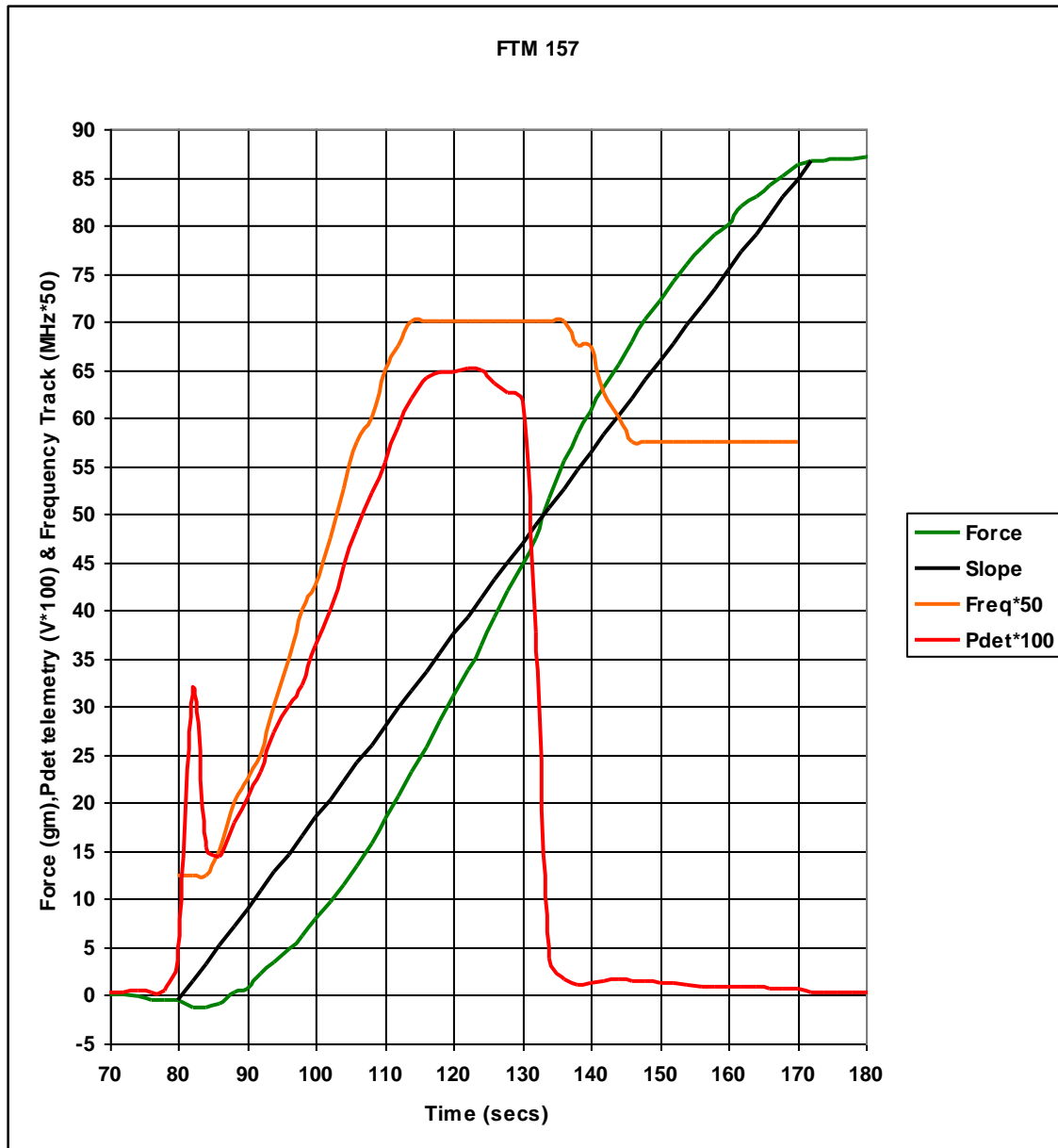


Fig 6.5 FTM 157 Test Results

Proprietary Information

The results of FTM 157 are shown in fig 6.5. This shows an increase in Pdet corresponding to the increase in frequency, given in the frequency track plot. Pdet reaches a maximum around 115 secs. The reaction force, given by the difference between the force and the slope plots has already peaked (around 105 secs) and is decreasing as loss of resonance approaches. Loss of resonance occurs at 130 secs, and is shown by a sharp drop in Pdet. The subsequent decrease in frequency does not recover resonance, due to the feedback effect of a drop in temperature at the input loop, as the high resonance current drops, and the reflected power increases.

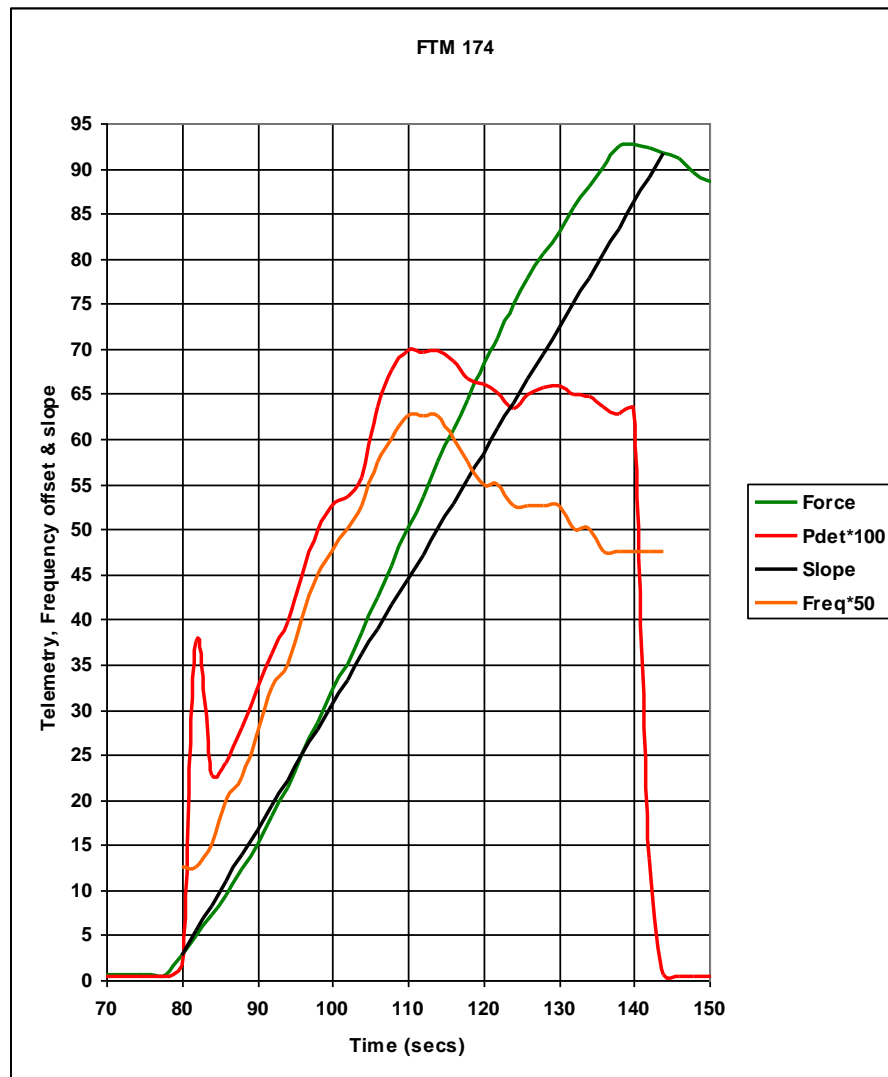


Fig 6.6 FTM 174 Test Results

The results of FTM 174 are shown in fig 6.6 and 6.7. Fig 6.6 shows a frequency increase which leads to maximum Pdet being achieved by 110 secs. The frequency is then stepped down, as the cavity expansion effect takes over from the input circuit warm up, and resonance is tracked until the power is turned off around 140 secs. Note that the criteria for minimum P_{refl} was 70mV for test FTM 174, whereas in test 157 it was allowed to drop below

Proprietary Information

20 mV. The resulting Reaction Force plot is given in fig 6.7, together with Pdet and Prefl plots.

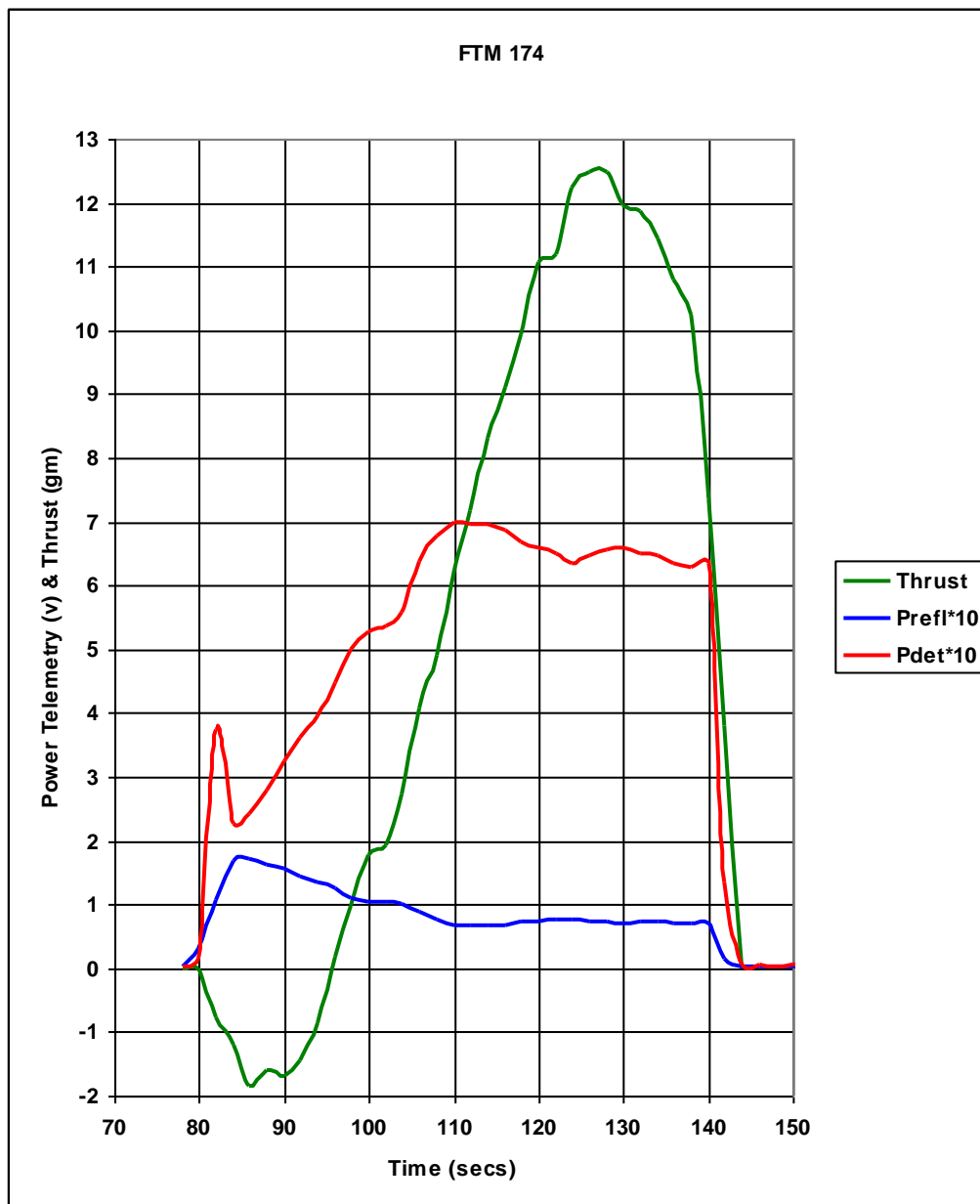


Fig 6.7 FTM 174 Test Results

6.4 Thermal results and analysis

Fig 6.8 shows the temperature data for FTM 154, a medium power test run. The EMC effect on temperature data can be clearly seen on the ambient results. The highest temperature rise can be seen in the input and top plate

Proprietary Information

temperatures. The main contribution to the input temperature rise is the loss in the input cable.

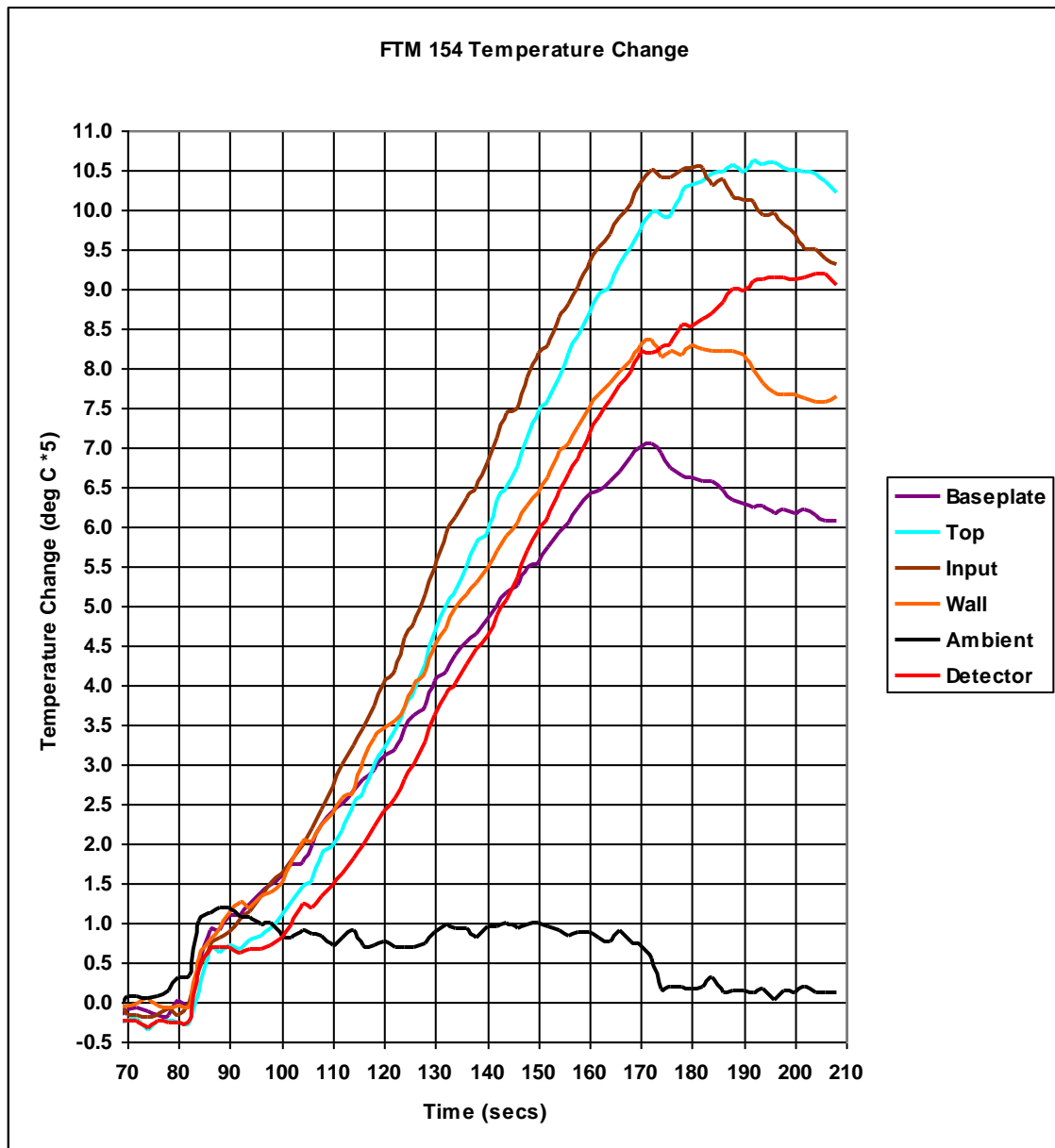


Fig 6.8 Temperature Change Data for FTM 154

The high top plate temperature compared, to the baseplate temperature is consistent throughout the test programme. This did not, at first, seem to correlate with theory, as a higher baseplate loss occurs, due to the larger baseplate radiation force, compared to the top plate.

Proprietary Information

However by taking into account the differences between the dissipating and radiating areas, for both top and bottom plates, and using the Design Factor, from the design software, to determine the ratio of losses at each plate, a predicted temperature ratio could be calculated. For the Flight Test Model this ratio was calculated to be 0.66.

The temperature data for each of the 19 performance tests was then corrected for EMC effects, and used to calculate a mean ratio between measured baseplate and top plate temperature changes. The mean ratio was 0.69, with a Standard Deviation of 0.03. This is a very close agreement between the predicted and measured temperature ratios, for baseplate and top plate.

The temperature data was also used to give a plot of baseplate temperature change against input power, and is shown in fig 6.9. This shows the expected linear increase in temperature change, with increased power.

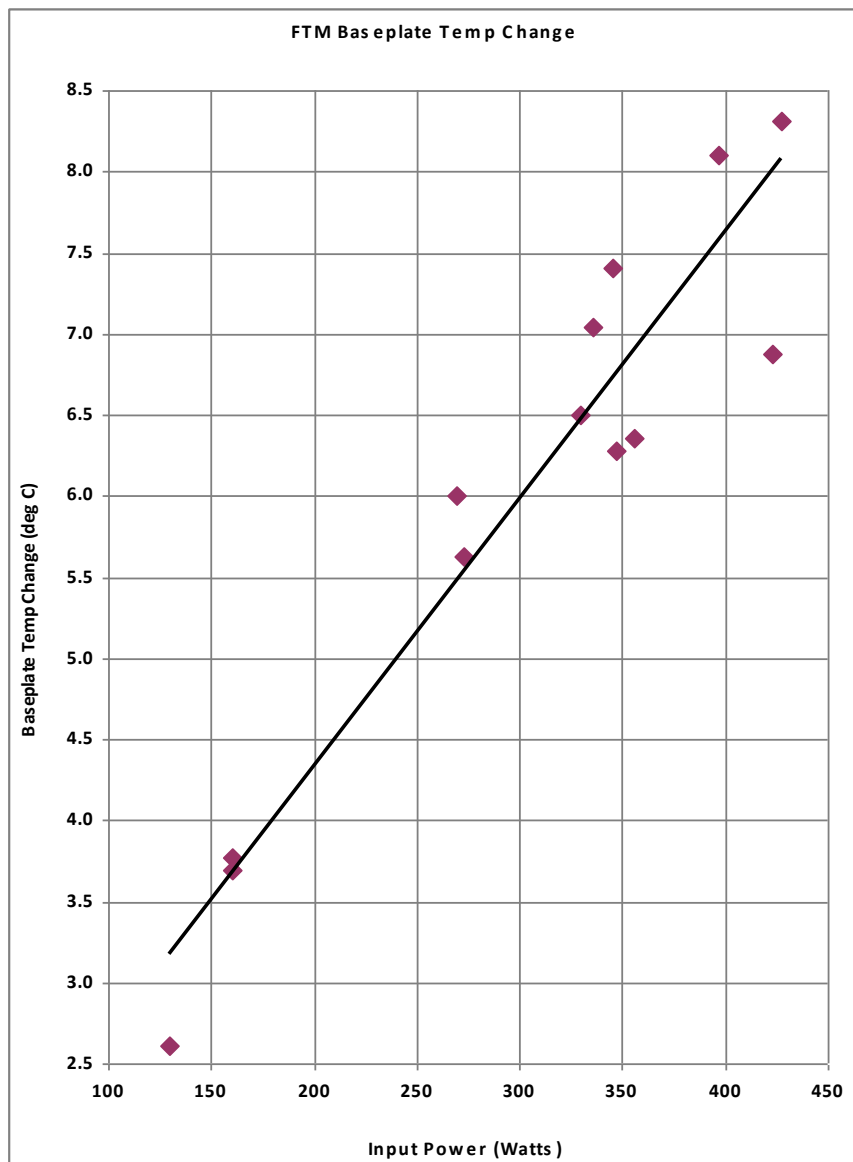


Fig 6.9 Baseplate Thermal Results

Proprietary Information

Prior to each test run, the resonant frequency was measured for the initial wall temperature of the cavity. The resulting data is plotted in fig 6.10, and shows the expected linear decrease in frequency with increased wall temperature, due to the increased path length.

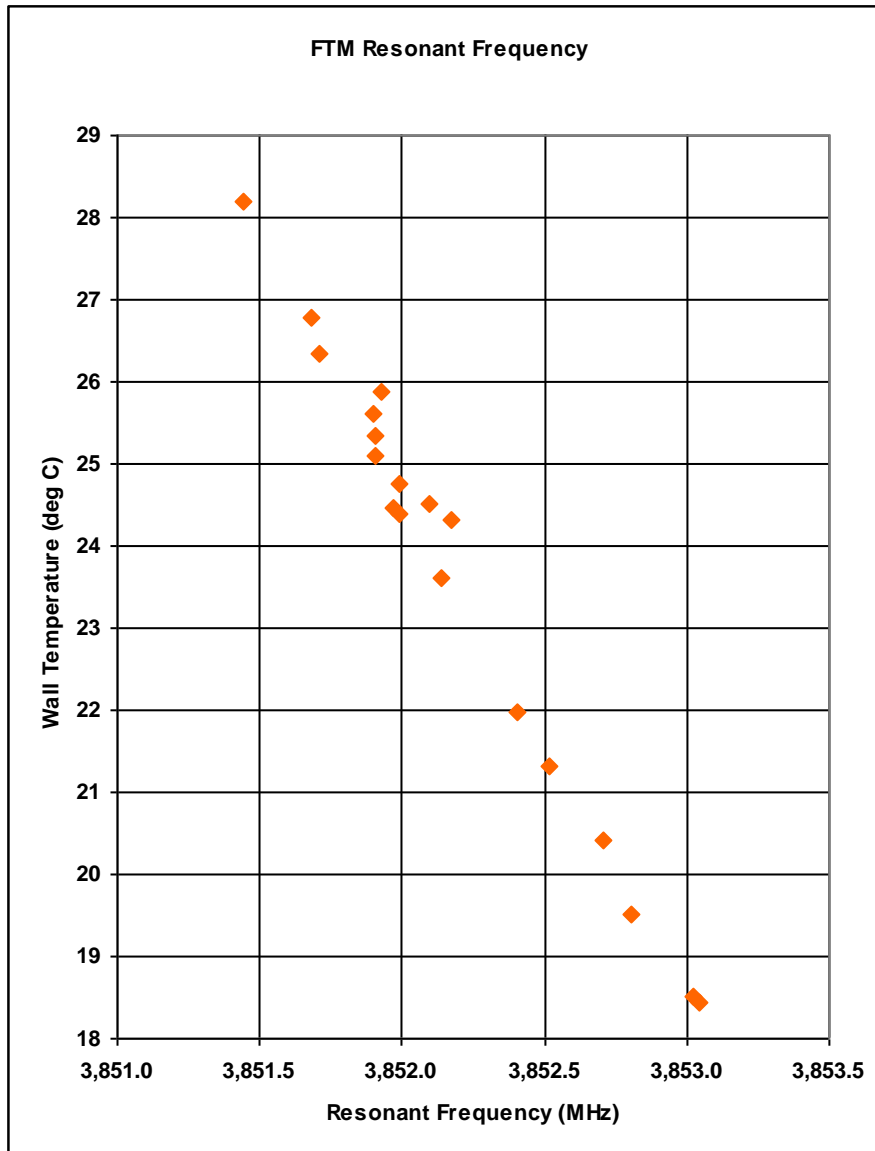


Fig 6.10 Wall temperature / Resonant Frequency Plot

The mean temperature coefficient from this data is -0.164 MHz/deg C

Using the design software, the resonant frequency shift was calculated over the 10 degree temperature range of the test data. This gave a calculated temperature coefficient of -0.184 MHz/deg C, which is in good agreement with the test data.

Proprietary Information

7. Test Summary and Conclusions

Table 6 gives the key parameters of the Flight Test Model thruster, and compares the values predicted from the design process, and those measured under test.

| Parameter | Design | Test |
|--|---------------|-------------|
| Operating Frequency (MHz) | 3,873.6 | 3,850.7 |
| Max Theoretical Q | 73,243 | |
| Unloaded Q | | 55,172 |
| Specific Thrust (mN/kW) (Calculated from the measured unloaded Q) | 301 | 326 |
| End Plate Temperature Ratio | 0.66 | 0.69 |

Table 6 Test Results Summary

Using the Design Software, the resonant frequency at a nominal 20 °C was predicted to be 3873.6 MHz, from the nominal dimensions. The actual measured resonant frequency was 3850.7 MHz. The lowering of the resonant frequency has been noted on previous thrusters, and is attributed to the effect of the input loop, together with a detailed modification to the nominal geometry of the cavity, carried out to increase unloaded Q.

The theoretical maximum Q for the cavity is calculated as 73,243 and as with all previous thrusters, the measured unloaded Q falls well below this at 55,172. The main reason for the discrepancy is the effect of dimensional tolerance on wavefront distortion, which is discussed in Section 2.3.

A secondary effect, is the slight loss introduced into the cavity, by the detector used to measure the Q. This has no effect on the actual unloaded Q, as it is part of the external equivalent circuit, as discussed in section 6.2. However the measured unloaded Q will always be below the actual unloaded Q, and gives rise to a lower predicted specific thrust. This is considered to be a contributor to the lower predicted specific thrust of 301 mN/kW, compared to the mean figure given by the test data of 326mn/kW.

Finally, table 6 gives the predicted end plate temperature ratio of 0.66, compared to the measured mean value of 0.69. This data provides a purely thermal confirmation of the design process.

Thus the test programme has validated the Flight Test Thruster design by electrical measurement, by mechanical measurement and by thermal measurement. It therefore enables this thruster design, to be put forward for a full flight qualification programme.

8. Appendix A.

This appendix contains the original manufacturing drawings, which illustrate the internal shaping of the baseplate, necessary to minimise phase distortion across the wavefront, (see Drgn FTM1 005).

Also included is a drawing showing the cavity modifications necessary to correct for a baseplate profile error, (see Drgn FTM1 009). These modifications increased the measured unloaded Q from 31,680 to 50,654.

The final measured unloaded Q of 55,172 was achieved with careful shimming between the baseplate and the body flange to compensate for machining tolerances.

CONTENTS

Drgn FTM1 001 issue 2. C Band Cavity Assembly.

Drgn FTM1 002 issue 2. C Band Cavity General Arrangement.

Drgn FTM1 003 issue 2. Input Loop Assembly.

Drgn FTM1 004 issue 2. C Band Cavity Body.

Drgn FTM1 005 issue 1. C Band Cavity Baseplate.

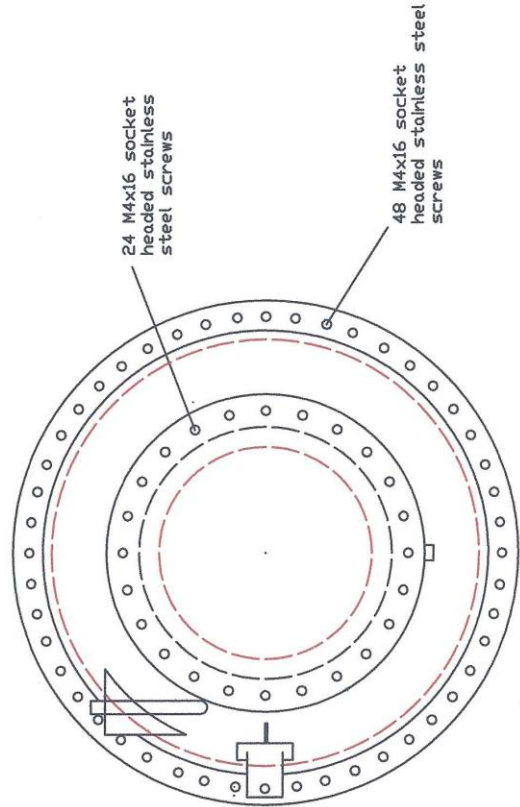
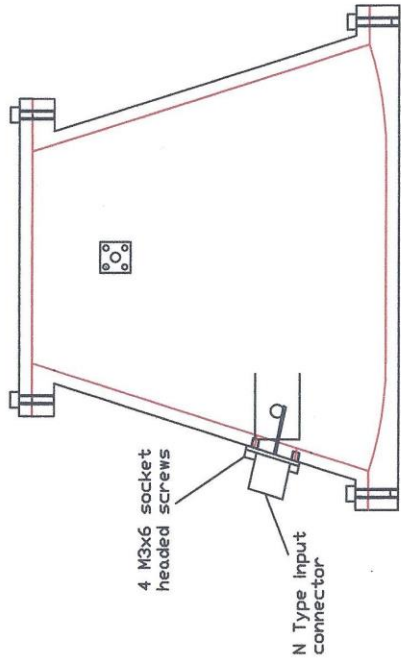
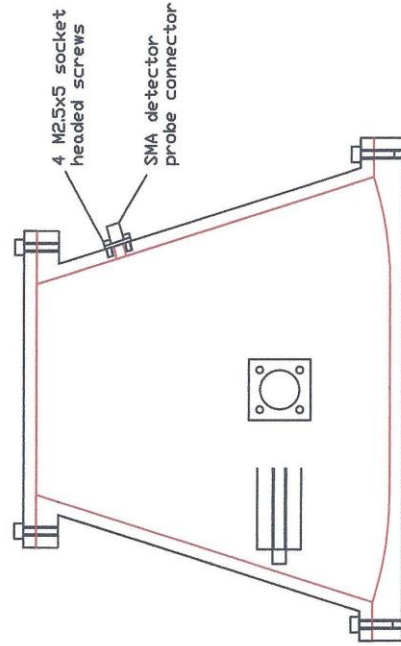
Drgn FTM1 006 issue 2. C Band cavity Top Plate.

Drgn FTM1 007 issue 2. Input Mounting Detail.

Drgn FTM1 008 issue 2. Detector Mounting Detail.

Drgn FTM1 009. C Band Cavity Modification.

SPR Ltd PROPRIETARY INFORMATION

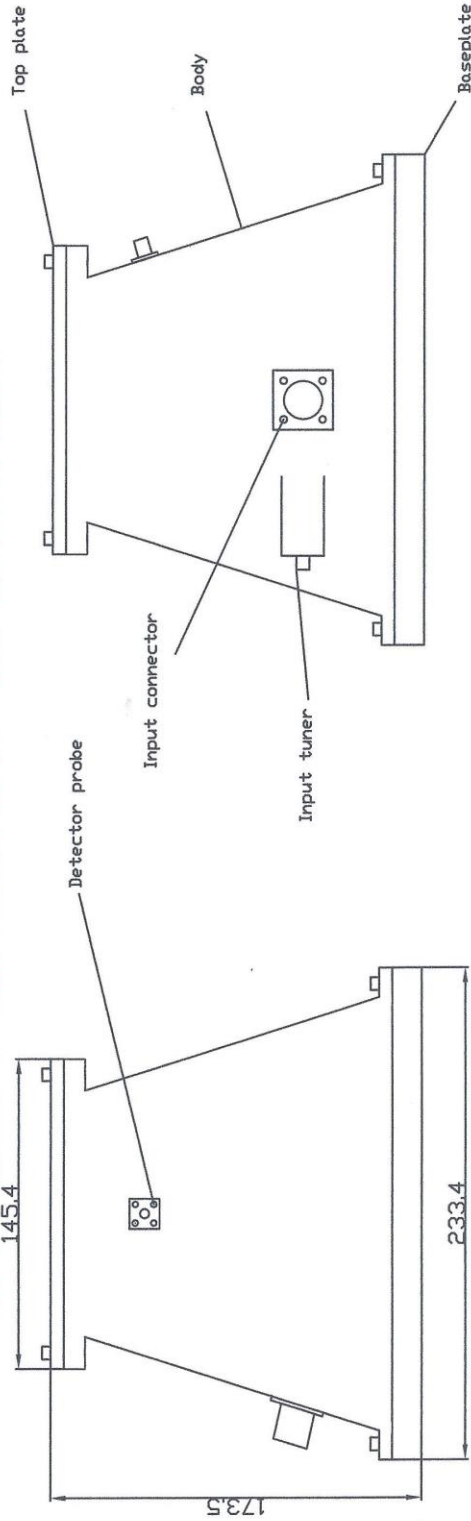


Dimensions mm

| | | |
|------------|--------------|--------------------------|
| Tolerances | Internal | +/-0.05mm |
| | External | +/-0.1mm |
| Material | AlMgSI Alloy | |
| Finish | Internal | Polished & silver plated |
| | External | Machined |

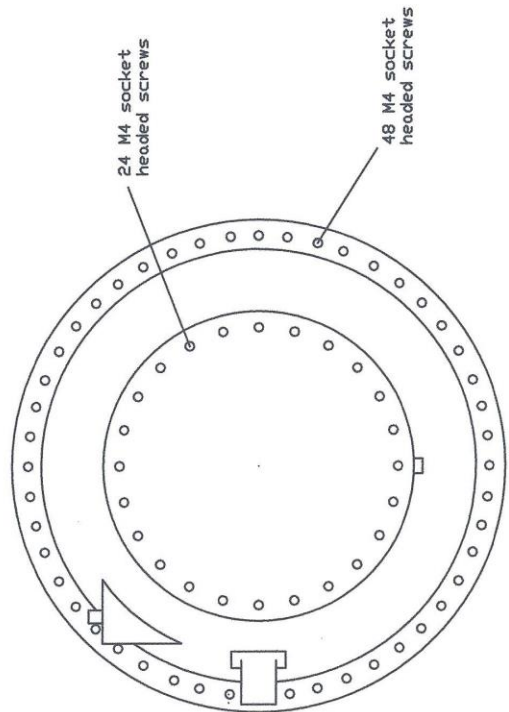
SPR Ltd
C Band Cavity Assembly
Drgn FTM1 001 issue 2

SPR Ltd PROPRIETARY INFORMATION

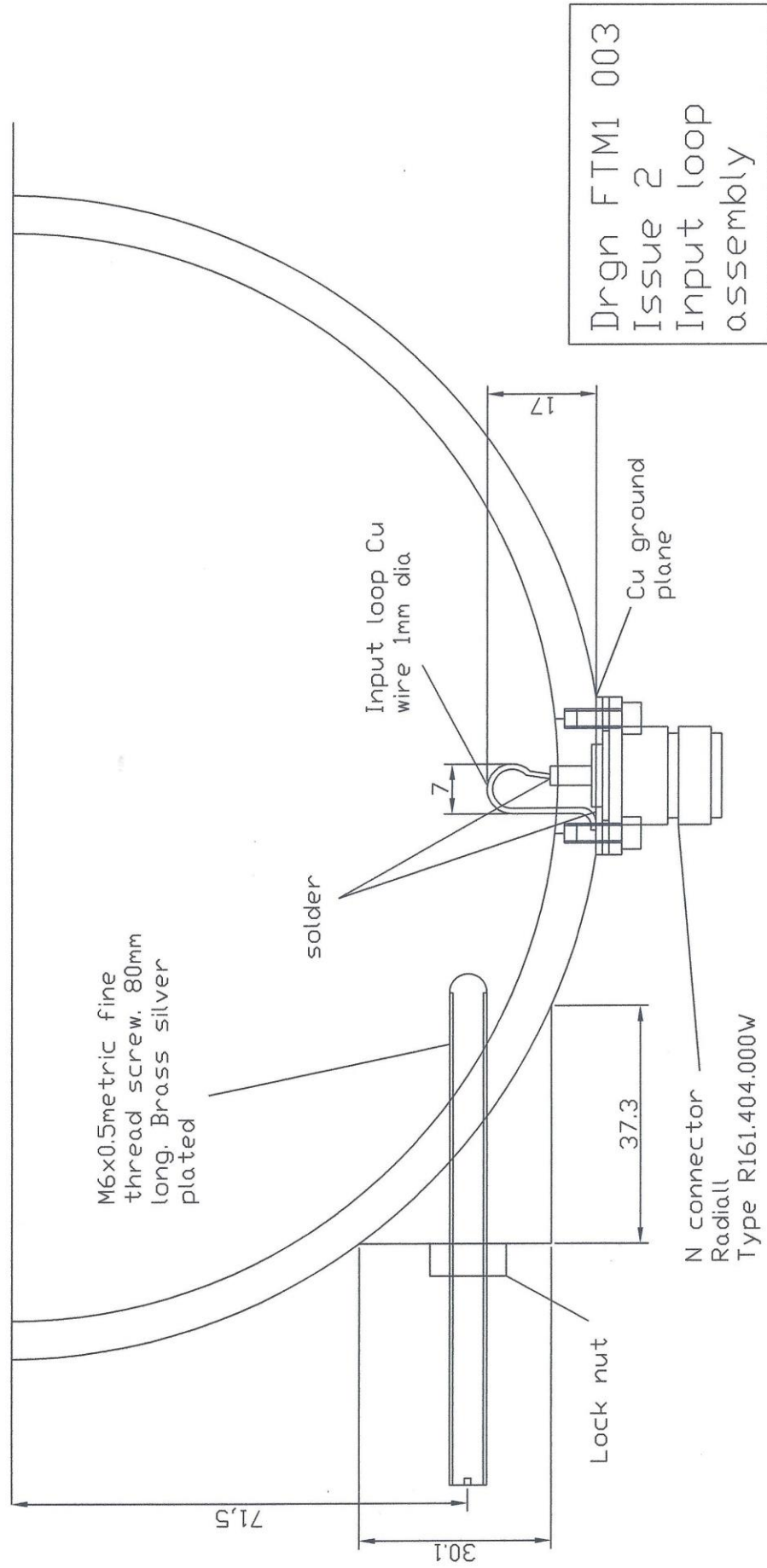


Dimensions mm
 Tolerances Internal +/-0.05mm
 External +/-0.1mm
 Material AlMgSi Alloy
 Finish Internal - Polished & silver plated
 External - Machined

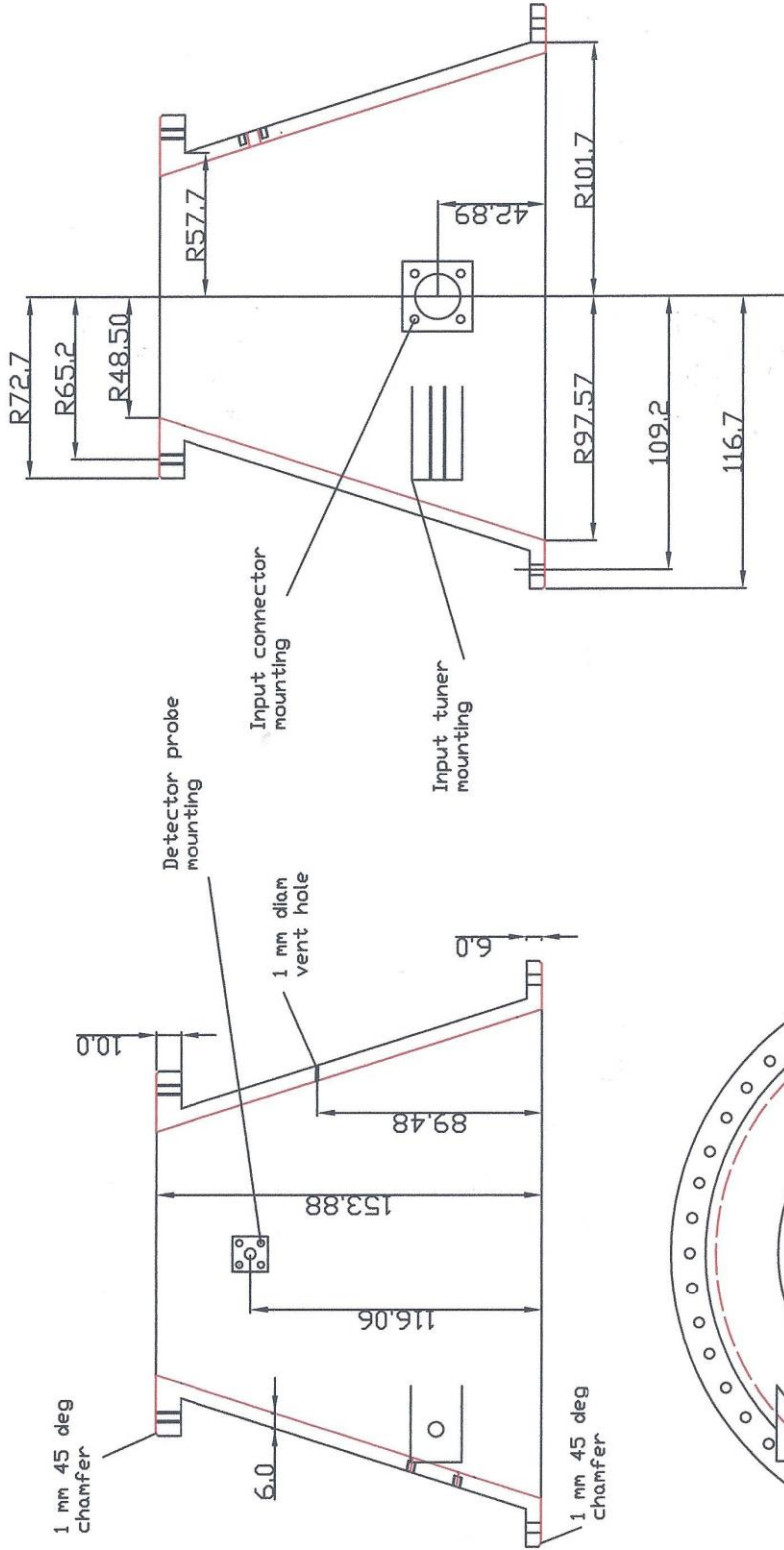
SPR Ltd
 C Band Cavity
 General Arrangement
 Drgn FTM1 002 Issue 2



SPR Ltd PROPRIETARY INFORMATION



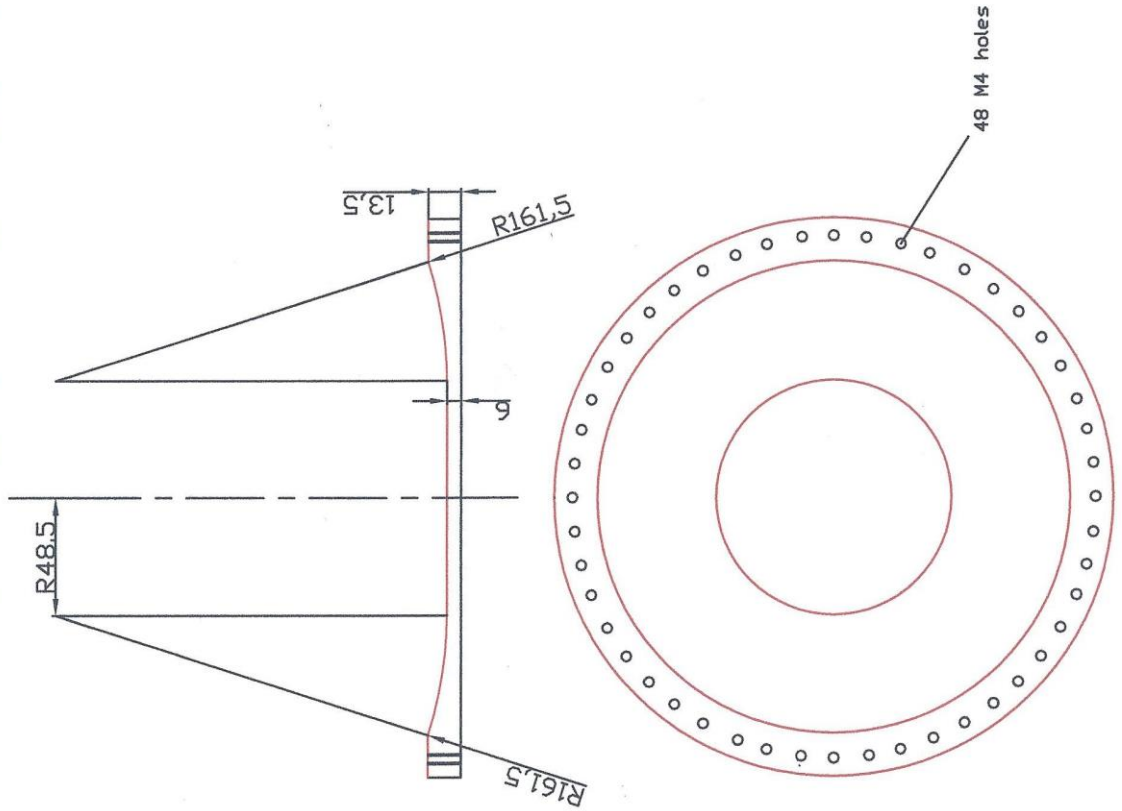
SPR Ltd PROPRIETARY INFORMATION



Dimensions mm
 Tolerances Internal +/-0.05mm
 External +/-0.1mm
 Material AlMgSi Alloy
 Finish Internal Polished & silver plated
 External Machined

SPR Ltd
 C Band Cavity Body
 Drgn FTM1 004 issue 2

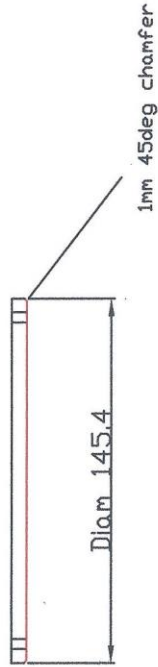
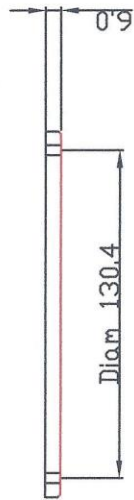
SPR Ltd PROPRIETARY INFORMATION



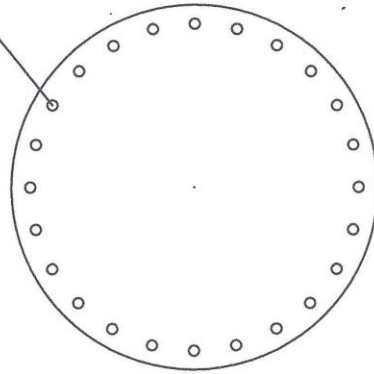
Dimensions mm
 Tolerances Internal ± 0.05 mm
 External ± 0.1 mm
 Material AlMgSi Alloy
 Finish Internal Polished & silver plated
 External Machined

SPR Ltd
 C Band Cavity Basplate
 Drgn FTM1 005 issue 1

SPR Ltd PROPRIETARY INFORMATION



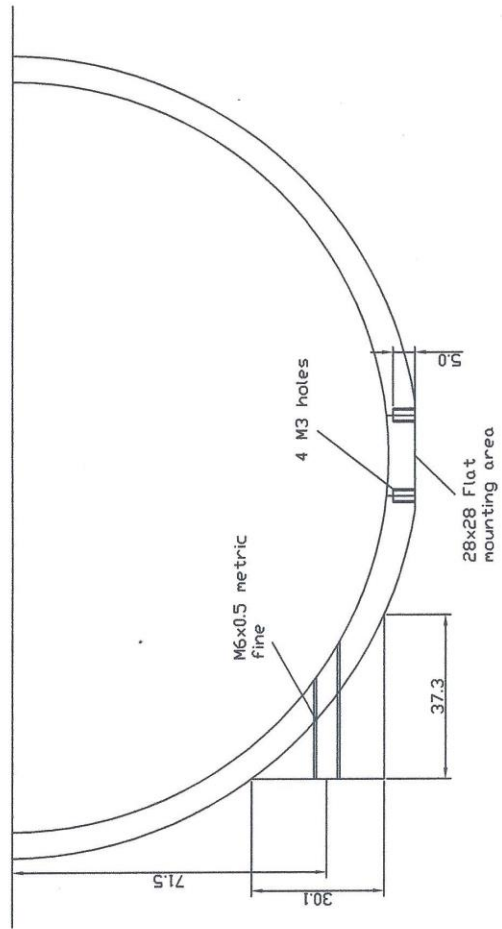
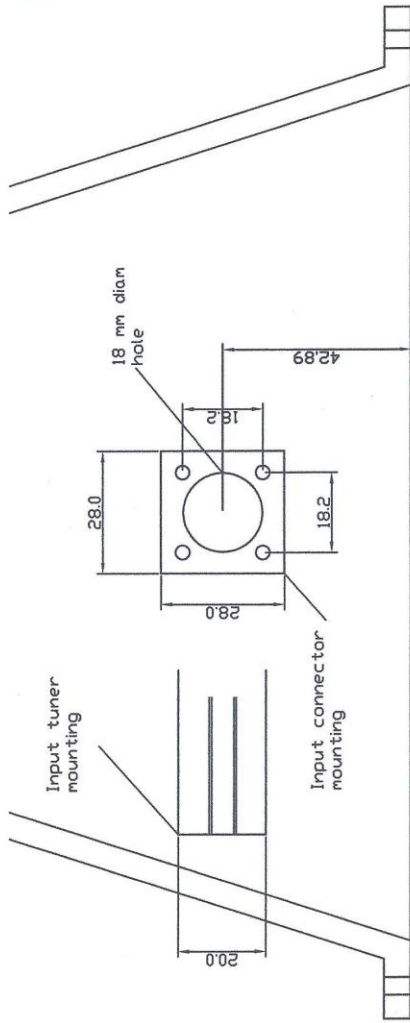
24 holes 4.2mm diam



Dimensions mm
Tolerances Internal $\pm 0.05\text{mm}$
External $\pm 0.1\text{mm}$
Material AlMgSi Alloy
Finish Internal Polished & silver plated
External Machined

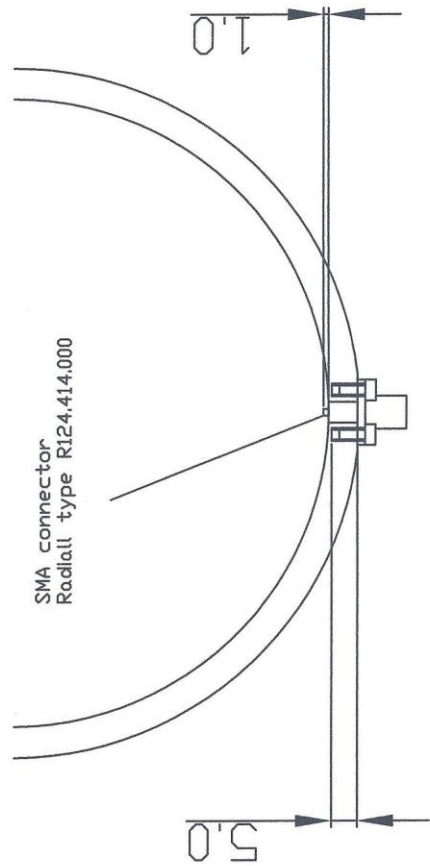
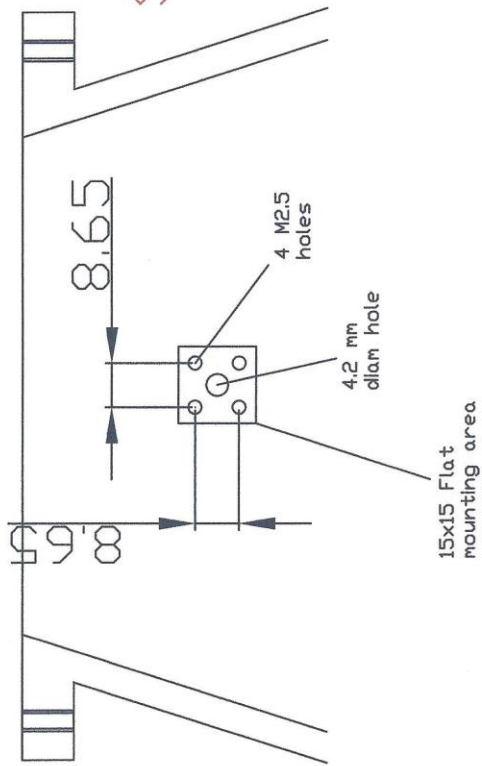
SPR Ltd
C Band Cavity
Top plate
Drgn FTM1 006 issue 2

SPR Ltd PROPRIETARY INFORMATION



Drgn FTM1 007
Issue 2
Input mounting
detail

SPR Ltd PROPRIETARY INFORMATION



SPR Ltd
Detector mounting
detail
Drgn FTM1 008 issue 2

SPR Ltd PROPRIETARY INFORMATION

SPR Ltd
C Band Cavity
Modification
Drgn FTM1 009

NOTE Baseplate profile error and
modification discs shown X10 scale

